Effects of Central Elements on the Properties of Group 13 Dialdiminate Complexes

*Yuto Aoyama, Yuki Sakai, Dr. Shunichiro Ito and Prof. Dr. Kazuo Tanaka**

Department of Polymer Chemistry, Graduate School of Engineering, Kyoto University
Katsura, Nishikyo-ku, Kyoto 615-8510, Japan

Email: tanaka@poly.synchem.kyoto-u.ac.jp
Homepage URL: https://poly.synchem.kyoto-u.ac.jp/en/

Abstract

Novel luminescent dialdiminate complexes of the group 13 elements were prepared to evaluate the effects of the central element on their properties. We demonstrate that their absorption wavelength and the response to Lewis bases apparently depend on the central atom. The aluminum complex exhibited the absorption band in the higher-energy region than the gallium and indium congeners. Theoretical calculations suggest that the aluminum complex has a lower-lying highest-occupied molecular orbital than the other complexes. Additionally, the emission intensity of the aluminum complex clearly changed in response to a Lewis base. Quantum chemical calculations suggest that these element-dependent optical properties could originate from the difference in the electric charges on the central elements. Interestingly, the ligand exchange reactions were observed in the indium complexes together with the changes in the optical properties and controlled by the addition of $InCl_3$ and $InMe_3$. Furthermore, all the complexes showed the aggregation-induced emission enhancement (AIEE) and crystallization-induced emission enhancement (CIEE) properties. These results lead to proposing a practical strategy for manipulating the optoelectronic properties coupled with the reactivities of complexes by choosing the central elements in the same group.

Introduction

Group 13 elements have a vacant p orbital, enabling the formation of various functional complexes involving luminescent dyes[1] and n-type semiconducting compounds.[2] Their optoelectronic functions of metal complexes can be modulated by modifying ligands, changing coordination numbers, and incorporating them into polymer chains.[1c] These strategies have allowed us to achieve advanced properties such as near-infrared absorption and emission,[3] stimuli-responsive luminescence,[4–7,15f] and thermally activated delayed fluorescence.[8] In addition to these typical strategies, alteration of the type of element at the coordination center in the same group has also attracted growing attention as an intriguing way to modulate the chemical properties of complexes. Recently, it has been demonstrated that the element alteration of complexes enables us to modulate their optical,[9] catalytic,[10] photophysical,[11,12] and stimuli-responsive luminescence properties.[4] However, there are still limited examples of systematic studies on the effects of the elements on the excited-state properties of the complexes, probably because the heavier-element complexes tend to be less stable under the measurement conditions than the lighter-element congeners.[12] Moreover, in some cases, that is likely because the syntheses of the complexes of each element were reported independently.[13]

β-Diketiminate ligands, involving two nitrogen atoms as the coordination sites of the chelating ligands, have been utilized to stabilize not only the group 13 complexes[15a] but also other highly reactive complexes.[14] The tunability of their steric and electronic demands by the substituents on the nitrogen atoms makes it possible to isolate such unstable species. Our group has recently reported that the *β*-diketiminate complexes of the group 13 elements exhibit superior properties such as aggregation-induced emission (AIE), CIEE, mechanochromism, and vapochromism.[15b–d] It was implied that the electronic structures could be changed by altering the central atoms.[15e] However, there is still plenty of room for clarifying the effects of the group 13 elements on the photophysical properties of the complexes and their origins. In this context, the fact that these *β*-diketiminate complexes hardly emit in diluted conditions has hampered us from unveiling the single-molecule properties and discussing the detailed mechanism of the differences in properties.

Herein, we report the synthesis of a novel series of group 13 complexes with a *β*-dialdiminate ligand and their photophysical properties. Importantly, these complexes exhibited fluorescence in both solutions and solids, in stark contrast to the *β*-diketiminate analogs. In addition, all synthesized complexes showed both the AIEE and CIEE properties accompanied by changes in the emission maxima. Comparing their

photophysical properties, the differences in the absorption maxima and the response to Lewis bases were observed. Theoretical calculations suggest that the difference in the electric charge on the central atom could be responsible for the different photophysical properties. Interestingly, the ligand exchange reactions of the indium complexes occurred together with the changes in the optical properties. The addition of $InCl_3$ and $InMe_3$ enabled us to reversibly control the exchange reactions.

Results and Discussion

Synthesis and Characterization of the Complexes

The dialdiminate ligand (**2**) was synthesized from the corresponding vinamidinium salt **1** according to the previous report, as shown in Scheme 1.[16] Aluminum and indium dialdiminates, **PhAlMe** and **PhInMe**, were prepared by the reaction with the corresponding trimethyl species ($AlMe_3$ or $InMe_3$) and the ligand **2**. **PhGaMe** was synthesized by the complexation of **2** with $GaCl_3$ to give a dichlorogallium complex **PhGaCl**, followed by the methylation by methyllithium. The chemical structures of the compounds were confirmed by ^1H and $^{13}C\{^1H\}$ NMR spectroscopy, high-resolution mass spectrometry (HRMS), and single-crystal X-ray diffraction (SCXRD) (Figures S1–S9, S21–S23). The spectroscopic data for **1**, **2**, **PhAlMe**, and **PhGaMe** were consistent with

the expected ones and characterized as pure compounds. Meanwhile, the ^{1}H NMR spectrum of the solution of the X-ray-quality **PhInMe** crystal showed minor peaks inconsistent with the chemical structure of **PhInMe**. In the ^{1}H NMR spectra, the ratio of the minor and major peaks in the imine region (7.88–8.01 ppm) was 1:4, while that in the methyl region (–0.13–0.33 ppm) was 0.5:4. These results suggest that the minor species corresponded to **PhInMeCl**, which has the single methyl group on indium (Scheme 2). HRMS with the method of direct analysis in real time (DART) was carried out for both solution and crystalline samples. Accordingly, it was indicated that **PhInMeCl** was detectable only in the solutions. The result of the SCXRD analysis revealed that the X-ray-quality crystal was composed only of **PhInMe**. These observations suggest that the dissolution of the crystal should afford the **PhInMeCl** via the equilibrium with a trace amount of unremovable by-products such as $InMe_nCl_{(3–n)}$ (n = 1–3), which should be concomitantly generated in the methylation of $InCl_3$, as shown in Scheme 2. Indeed, the hydrolyzed dimer $(InMe_2\text{-}\mu O)_2$, corresponding to $InMe_2Cl$, was detected in the HRMS of the solution.

Scheme 1. Synthetic scheme of group 13 dialdiminate complexes

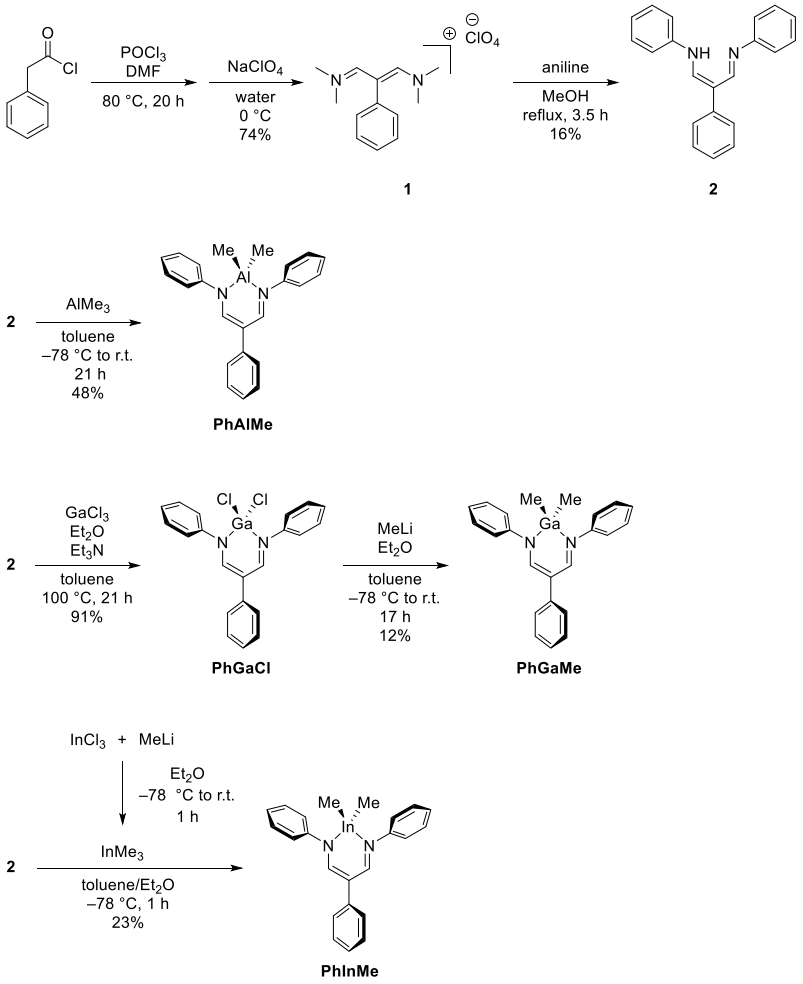

Scheme 2. Plausible mechanism for the generation of the monochloroindium complexes in the solution state

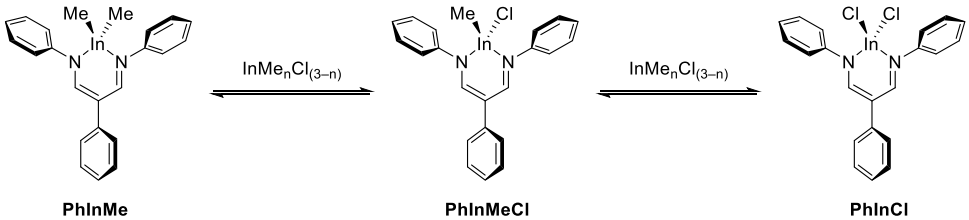

Ligand Exchange Reaction of PhInMe

In order to evaluate the equilibrium among the indium complexes as shown in Scheme 2, the reactions of the indium dialdiminate complexes with $InCl_3$ and $InMe_3$ were

monitored by ^{1}H NMR and optical measurements. When a saturated $InCl_3$ solution in CD_2Cl_2 was added to the **PhInMe** solution, ^{1}H NMR spectra showed that the major peak (7.88 ppm) assigned to **PhInMe** decreased with an increase in the amount of $InCl_3$ solution (Figure 1a). When an excess amount of the $InCl_3$ solution was added, the original peaks completely disappeared. Besides, two distinct peaks increased with the reaction with $InCl_3$: One was derived from **PhInMeCl** (8.04 ppm), which was also detected as the minor peak in the pristine solution; the other is attributed to **PhInCl** (8.11 ppm) confirmed by HRMS, which was initially absent. These observations justified the reaction mechanism for the chlorination of **PhInMe**, as shown in Scheme 2. Conversely, the addition of a saturated $InMe_3$ solution to the pristine **PhInMe** solution led to an increase in the amount of **PhInMe**. The excess addition allowed the vanishment of the minor peaks from **PhInMeCl**. Consequently, the methylation of the **PhInMeCl** to **PhInMe** also should proceed by the reaction with $InMe_3$. Importantly, it was demonstrated that a solution of **PhInMe** without any other dialdiminate complexes can be obtained in the presence of an excess amount of $InMe_3$. Based on this result, the properties of a **PhInMe** solution itself were evaluated under this condition in this paper.

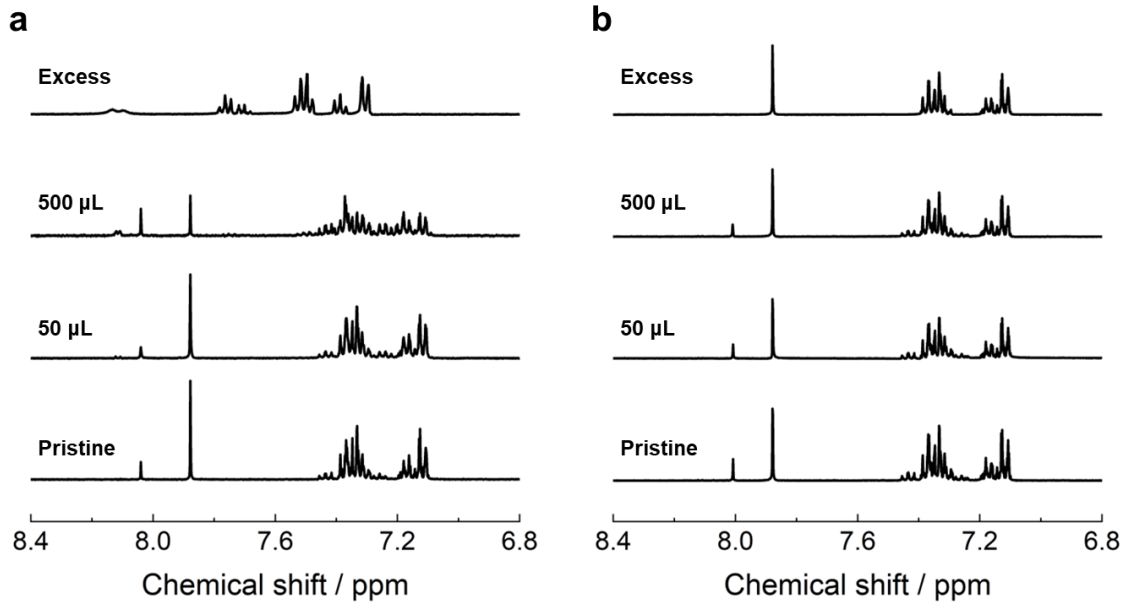

Figure 1. ^{1}H NMR spectra of **PhInMe** in CD_2Cl_2 with the different amounts of saturated solutions of (a) $InCl_3$ and (b) $InMe_3$.

The reactions between the indium dialdiminate complexes were also monitored by optical measurements (Table S1). The pristine CH_2Cl_2 solution of the **PhInMe** crystals, containing a small amount of **PhInMeCl**, showed the absorption maxima at 435 nm. The addition of the $InCl_3$ solution resulted in the disappearance of the initial absorption band and the increase of the new band peaked at 395 nm (Figure 2a). The excess addition of $InCl_3$ to the solution of **PhInMe** crystal resulted in the blue shift of the absorption maxima to 392 nm (red line in Figure 2c). Similarly, the $InCl_3$ addition weakened the initial emission peak at 511 nm and magnified the broader band at 470 nm (Figure 2b). When the $InCl_3$ solution was excessively added, the emission peak reached 488 nm (red line in Figure 2d). Conversely, the excess addition of $InMe_3$ resulted in the red shift of the

absorption peak from 435 nm to 443 nm, although the emission peak hardly shifted (blue lines in Figures 2c and 2d). The reversibility of the optical properties was also confirmed by the subsequent addition of $InCl_3$ and $InMe_3$, and *vice versa* (Figures S10 and S11).

The origin of the shifts in the absorption and emission bands was evaluated by the density functional theory (DFT) and time-dependent DFT (TD-DFT) calculations for the three indium complexes at the PBE1PBE/6-31G(d,p) (for C, H, N, and Cl) and LanL2DZ (for In) level of theory (Table 1) with the Tamm–Dancoff approximation (TDA) using Gaussian 16 Rev. C01.[17] The calculated S_0–S_1 electronic transition energy of **PhInMe** was significantly smaller than that of **PhInCl**. This is consistent with the experimental results. The calculation data indicated that the S_1 states of these complexes are mainly composed of the transition between their highest-occupied and lowest-unoccupied molecular orbitals (HOMO and LUMO). In addition, the HOMOs of the complexes were significantly distributed to the monodentate ligands, while the LUMOs had a nodal plane passing them. Therefore, the smallest HOMO–LUMO gap of **PhInMe** should be derived from the selective destabilization of its HOMO by the electron-donating character of the methyl groups. The red shift of the absorption maxima by adding the excess amount of $InMe_3$ should be caused by converting initially existing **PhInMeCl** into **PhInMe**. In

contrast to the absorption spectra, the emission spectra showed quite a little shift, probably because the energy transfer from **PhInMeCl** to **PhInMe** occurs in the initial state.

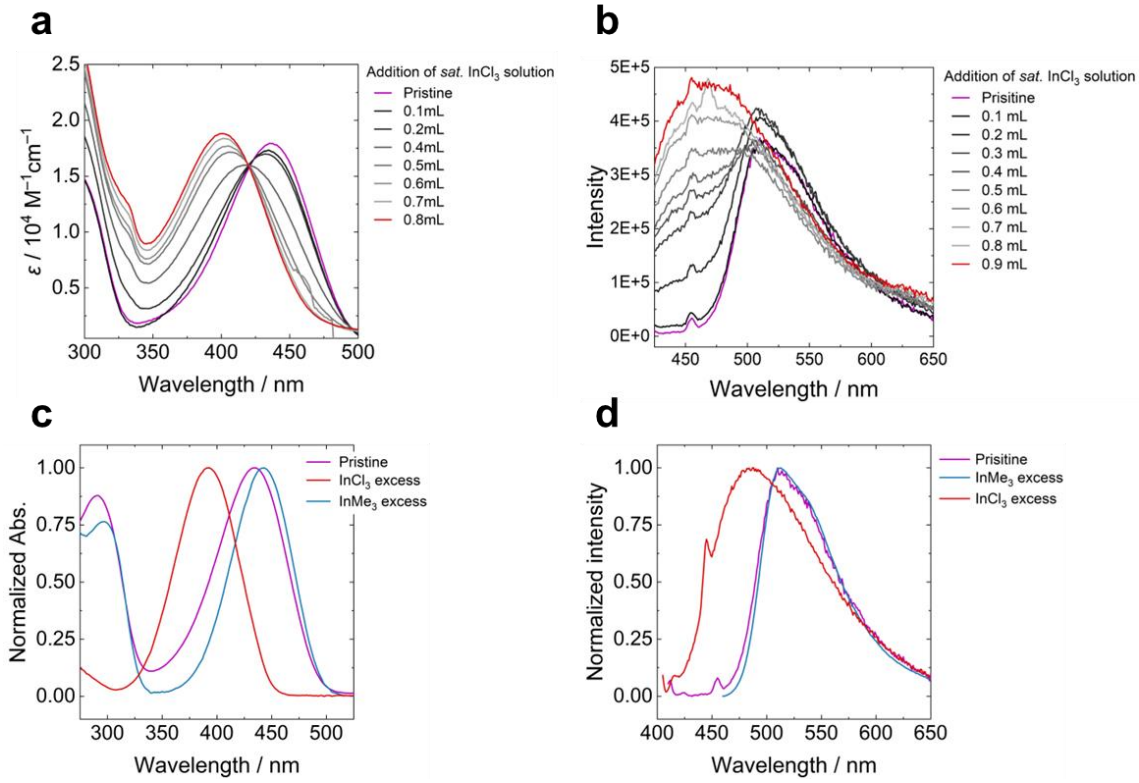

Figure 2. The changes in (a) absorption and (b) photoluminescence spectra when a sat. $InCl_3$ solution (in CH_2Cl_2) was added to 1.0×10^{-5} M solution of **PhInMe**. The changes in (c) absorption and (d) photoluminescence spectra when $InCl_3$ or $InMe_3$ was excessively added to 1.0×10^{-5} M solution of **PhInMe**.

Table 1. Calculated parameters of the electronic transitions at the S_0 state for single molecules [a]

	Composition [b]	Coefficient [c]	E / eV	λ / nm	f [d]

PhInCl	HOMO→LUMO	0.686	3.55 (3.92)	349	0.721
PhInMeCl	HOMO→LUMO	0.687	3.57 (3.94)	347	0.731
PhInMe	HOMO→LUMO	0.683	3.46 (3.87)	358	0.647

[a] Calculated at the level with PBE1PBE/6-31G(d,p) (for C, H, N, and Cl) and Lanl2DZ (for In). [b] Composition of the electronic states. [c] Coefficient for the electronic transition. [d] Oscillator strength.

Photophysical Properties of Dilute Solutions

To evaluate the electronic properties of the single molecules, the UV–vis absorption and photoluminescence spectra were measured for their dichloromethane solutions (1.0×10^{-5} M) as shown in Figure 3 and Table 2 (Figures S13–S15 and Tables S2–S4 for the other solutions). **PhAlMe** showed the absorption peak in the shorter-wavelength region than **PhGaMe** and **PhInMe** (λ_{abs} = 431 nm for **PhAlMe**, 441 nm for **PhGaMe**, and 443 nm for **PhInMe**). It is suggested that **PhAlMe** has a smaller energy gap between HOMO and LUMO than those of **PhGaMe** and **PhInMe** in their ground states. In contrast, all complexes exhibited emission peaks in almost the same region (λ_{em} = 515 nm for **PhAlMe**, 518 nm for **PhGaMe**, and 513 nm for **PhInMe**). This observation indicates that the central element should not significantly affect the HOMO–LUMO gap of their excited-state structures. Their absolute photoluminescence quantum yields (Φ_{PL}) in the solution

states were evaluated (Table 2). **PhGaMe** showed the highest quantum yield, while **PhInMe** showed the lowest one. The meager quantum yield of **PhInMe** could be attributed to the fast non-radiative deactivation probably due to its significant molecular motions, vibrations, and Lewis acidity. The relatively low quantum yield of **PhAlMe** in comparison with that of **PhGaMe** can also be explained by the larger non-radiative deactivation rate constant (k_{nr}) derived from the higher Lewis acidity rather than the change in radiative deactivation rate constant (k_r).

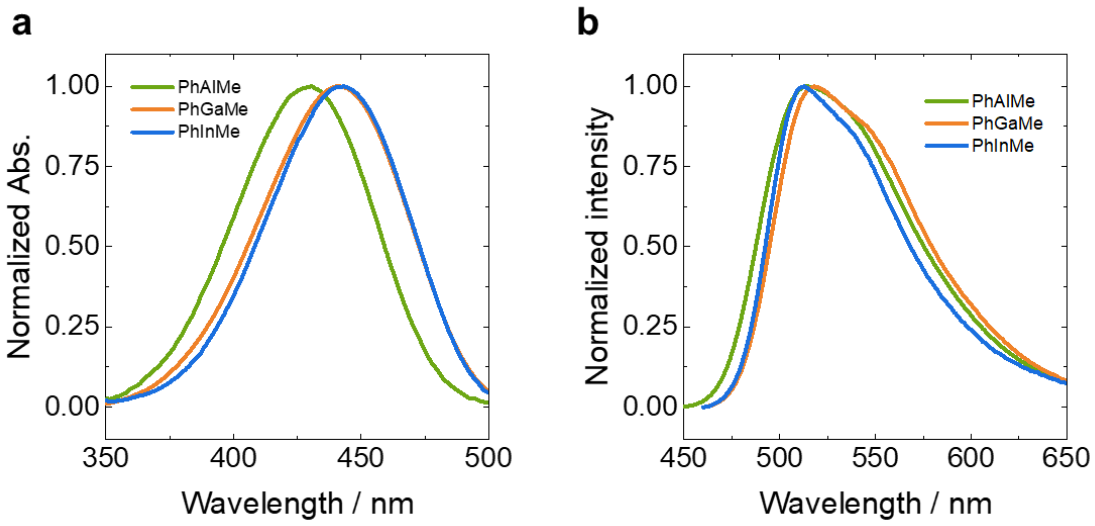

Figure 3. Normalized (a) UV–vis absorption and (b) photoluminescence spectra of the synthesized complexes in CH_2Cl_2 (1.0×10^{-5} M, PL: excited at each absorption maximum).

Table 2. Photophysical properties of the synthesized complexes in the dilute solutions

	λ_{abs} / nm	ε / 10^4 M^{-1} cm^{-1} [a]	λ_{PL} / nm [b]	Φ_{PL} [c]	k_r / 10^8 s^{-1} [d]	k_{nr} / 10^8 s^{-1} [d]
PhAlMe	431	1.9	515	0.087	1.6	17
PhGaMe	441	1.7	518	0.10	1.4	12
PhInMe	443	3.9	513	< 0.01	< 1.0	> 100

[a] Molar absorption coefficient at the absorption maxima. [b] Excited at λ_{abs}. [c] Determined with the integrated sphere method. [d] k_r and k_{nr} were determined from the following formula: $k_r = \Phi_{PL} / \langle\tau\rangle$ and $k_{nr} = (1 - \Phi_{PL}) / \langle\tau\rangle$, where $\langle\tau\rangle = \Sigma\alpha_i\tau_i^2 / \Sigma\alpha_i\tau_i = \Sigma f_i\tau_i$.

To discuss the differences in optical properties among the three complexes, especially in the absorption maxima, the quantum chemical calculations were carried out with DFT and TD-DFT methods at the PBE1PBE level of theory by utilizing TDA. Since the effective core potential (ECP) should be applied to the core shells of the indium atom, three complexes were not able to be compared directly with the same basis sets for all atoms. Therefore, the single-point calculations in the comparison between **PhAlMe** and **PhGaMe** were carried out with 6-31G(d,p) for C, H, N, Al, and Ga, while the calculation in the comparison between **PhGaMe** and **PhInMe** was performed with 6-31G(d,p) for C, H, and N and Lanl2DZ for Ga and In (Table 3). The S_1 states of all complexes were mainly composed of the HOMO–LUMO transitions. The largest S_0–S_1 electronic transition

energy was obtained from **PhAlMe** (3.41 eV, 364 nm) in good agreement with the experimental absorption spectra. Considering the HOMO and LUMO levels of the complexes, it is suggested that the selectively stabilized HOMO of **PhAlMe** leads to its largest HOMO–LUMO gap of **PhAlMe**. The methyl groups in all complexes significantly contributed to their HOMO, while their LUMO was located only at the dialdiminate moiety (Figure 4 and Tables 4 and S19–S22). Thus, the selective stabilization of the HOMO of **PhAlMe** might originate from the stabilization of the orbital energy of the methyl groups compared with those of **PhGaMe** and **PhInMe**. To get further insight into this mechanism, the partial charges on each atom in the molecules were calculated with the natural population analysis (NPA) with the optimized structures (Tables 4 and S15–S18). It was found that the aluminum atom in **PhAlMe** was more positively charged than the gallium and indium atoms in the other complexes in the same trend of electronegativity. These results suggest that the relatively positive aluminum atom might stabilize the electrons on the methyl groups more effectively than the gallium and indium atoms, resulting in its stabilized HOMO.

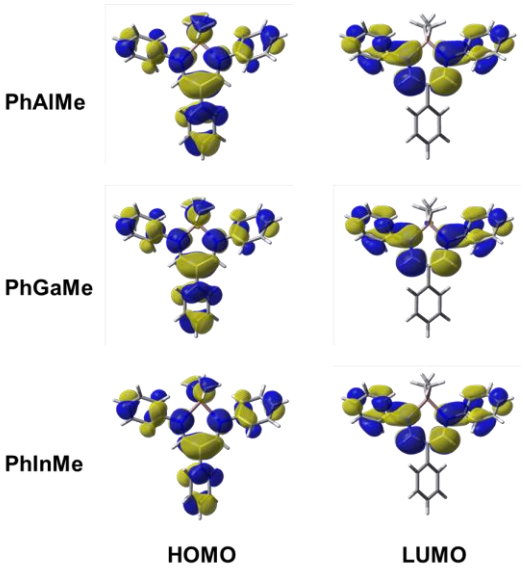

Figure 4. Orbital diagrams for the frontier molecular orbitals of the dialdimine complexes.

Table 3. Calculated parameters of the electronic transitions at the S_0 state for single molecules of **PhAlMe** and **PhGaMe** [a]

	Composition [b]	Coefficient [c]	E / eV	λ / nm	f [d]
PhAlMe	HOMO→LUMO	0.680	3.41	364	0.471
PhGaMe[e]	HOMO→LUMO	0.687 (0.687)	3.37 (3.42)	368 (362)	0.528 (0.564)
PhInMe	HOMO→LUMO	0.683	3.46	358	0.647

[a] Calculated at the level with PBE1PBE/6-31G(d,p) (for C, H, N, Al, and Ga) and Lanl2DZ (for In) unless otherwise noted. [b] Composition of the electronic states. [c] Coefficient for the electronic transition. [d] Oscillator strength. [e] Values in the parentheses were calculated with Lanl2DZ for Ga.

Table 4. Calculated electronic properties of **PhAlMe** and **PhGaMe**[a]

	Partial charge on central atom	Contribution from Me groups (%)	
		HOMO	LUMO
PhAlMe	1.84	4.0	0.14
PhGaMe[b]	1.58 (1.74)	3.3 (3.8)	0.10 (0.25)
PhInMe	1.74	3.3	0.15

[a] Calculated by NPA for the optimized structures of three complexes with PBE1PBE/6-31G(d,p) (for C, H, N, Al, and Ga) and Lanl2DZ (for In) unless otherwise noted. [b] Values in the parentheses were calculated with Lanl2DZ for Ga.

Response to Lewis Base

We envisioned that the intrinsic Lewis acidity of the four-coordinated group 13 element complexes would allow us to visualize the differences in the Lewis basicity of solvent molecules. Thus, the optical properties of the complexes were measured in the Lewis basic solvents. Acetonitrile (MeCN) and DCM were selected as Lewis basic and non-Lewis basic solvents, respectively. As mentioned earlier, the solution of the indium dialdiminate complex comprised a mixture of **PhInCl**, **PhInMeCl**, and **PhInMe**. Hence, the optical properties of **PhInMe** were not able to be quantitatively evaluated. The absorption and emission spectra of **PhAlMe** and **PhGaMe** in MeCN solutions differed

slightly from those in DCM solutions at room temperature (Table 5 and Figure S16). In addition, the photophysical properties show a less significant correlation with the solvent property (Figure S19). Meanwhile, as shown in Table 5, the quantum yields of **PhAlMe** and **PhGaMe** decreased in MeCN (0.087 in DCM and 0.03 in MeCN for **PhAlMe**, 0.10 in DCM and 0.04 in MeCN for **PhGaMe**). The k_{nr} values significantly increased as the quantum yields decreased, while the k_r values showed only a slight change. These results suggest that the non-radiative deactivation processes should be accelerated by interactions with the Lewis base, resulting in the decline in quantum yields. Although other Lewis basic solvents, such as tetrahydrofuran and pyridine, were also tested, significant data were not obtained due to the decomposition of the complexes in these solvents (Figures S13–S15).

Table 5. The optical properties of three complexes in the non-Lewis solvents and Lewis solvents

		λ_{abs} / nm	λ_{PL} / nm [a]	Φ_{PL} [b]	k_r / 10^8 s^{-1} [c]	k_{nr} / 10^8 s^{-1} [c]
PhAlMe	DCM (r.t.)	431	515	0.087	1.6	17
	MeCN (r.t.)	428	512	0.03	1.3	41

PhGaMe	2-MP (77 K)	449	482	0.98	1.8	0.046
	2-MTHF (77 K)	442	477	0.55	1.2	0.97
	DCM (r.t.)	441	518	0.10	1.4	12
	MeCN (r.t.)	440	514	0.04	1.1	25
	2-MP (77 K)	467	491	0.90	1.5	0.18
	2-MTHF (77 K)	464	489	0.87	2.1	0.31

[a] Excited at λ_{abs}. [b] Determined with the integrated sphere method. [c] k_r and k_{nr} were determined from the following formula: $k_r = \Phi_{PL} / \langle\tau\rangle$ and $k_{nr} = (1 - \Phi_{PL}) / \langle\tau\rangle$, where $\langle\tau\rangle = \Sigma\alpha_i\tau_i^2 / \Sigma\alpha_i\tau_i = \Sigma f_i\tau_i$.

The photophysical measurements in Lewis basic solvents were performed at cryogenic temperature to gain information about the mechanism of the response to the Lewis base,. 2-Methyltetrahydrofuran (2-MTHF) and 2-methylpentane (2-MP) were selected as Lewis basic and non-Lewis basic solvents used in cryogenic measurements, respectively. As well as the results at room temperature, the emission and excitation spectra in the 2-MTHF solution exhibited less significant differences from those in 2-MP at 77 K (Tables 5 and S5 and Figures S17 and S18). In contrast, the quantum yield of **PhAlMe** clearly

depended on the solvent, although it was not the case for **PhGaMe**. The quantum yield of **PhAlMe** in 2-MTHF solution (0.98) was about half lower than that in 2-MP (0.55). Along with the decrease in the quantum yield, the k_{nr} value was significantly increased. Considering that the molecular motions would be suppressed in the cryogenic state, the decrease in the quantum yield in Lewis basic solvents was ascribed to the non-radiative deactivation process resulting from the interactions with the Lewis base. In contrast to **PhAlMe**, the quantum yield and k_{nr} of **PhGaMe** were not influenced by the existence of the Lewis base. Notably, these differences in the responsiveness to the Lewis base between **PhAlMe** and **PhGaMe** should be derived from the difference in their Lewis acidity. As shown in Table 4, the aluminum atom in **PhAlMe** holds a more positive charge and could be more electrostatically interactive with Lewis bases than the gallium atom of **PhGaMe**.

Photophysical Properties in Solid States

It has been reported that diiminate complexes of group 13 elements show the AIE property.[15b–f] Hence, the photoluminescent properties of the dialdiminate complexes in their solid states were measured (Figure S20 and Table S6). All complexes exhibited higher photoluminescence quantum yields in the solid states than in the solution states,

indicating that these complexes have AIEE properties (Table 6). Photoluminescence lifetime measurements revealed that solidification led to a decrease in the k_{nr} values. These results mean that the AIEE properties should be derived from suppressing molecular motions and vibrations.[18] It is worth noting that the inter-chromophore interactions, such as π–π interactions, in the crystalline states can induce the bathochromic shift of their emission bands compared to the solution states. Nevertheless, such intermolecular interactions seem not to open significant non-radiative deactivation paths. Moreover, the quantum yields in the crystalline states of all complexes were larger than those in the amorphous states. The lower k_{nr} values in the crystalline states imply that the further suppression of molecular motions in their packing structures could be caused, followed by the enhancement of the quantum yields. Additionally, much lower energy emissions in the amorphous states suggest the existence of stronger intermolecular interactions that might cause the annihilation of excitons.

Table 6. The optical properties of three complexes in the solid states [a]

		λ_{PL} / nm [b]	Φ_{PL} [c]	k_r / 10^8 s^{-1} [d]	k_{nr} / 10^8 s^{-1} [d]
PhAlMe	Amorphous film	551	0.15	1.1	6.5

	Crystal	538	0.32	1.0	2.2
PhGaMe	Amorphous film	556	0.14	1.4	8.7
	Crystal	552	0.49	2.2	2.3
PhInMe	Amorphous film	550	0.016	0.38	23
	Crystal	560	0.30	0.83	1.9

[a] Amorphous samples were prepared on quartz substrates by the drop-casting method with the DCM solutions. [b] Excited at λ_{abs}. [c] Determined with the integrated sphere method. [d] k_r and k_{nr} were determined from the following formula: $k_r = \Phi_{PL} / \langle\tau\rangle$ and $k_{nr} = (1 - \Phi_{PL}) / \langle\tau\rangle$, where $\langle\tau\rangle = \Sigma\alpha_i\tau_i^2 / \Sigma\alpha_i\tau_i = \Sigma f_i\tau_i$.

To discuss the intermolecular interactions in the crystalline states, we carried out the single-point TD-DFT calculations for the monomeric and dimeric structures obtained from the single-crystal (SC) structures as well as the DFT-optimized structures (Figure 5 and Tables 7 and S10–S11). Compared with the optimized structures, the monomeric SC structure had higher HOMO and lower LUMO, thus showing the narrower HOMO–LUMO gap. The smaller dihedral angles between the aromatic rings and the central six-membered ring of the SC structure indicate that its structure should be more planar than

the DFT-optimized structure (Table 8). Therefore, the enhanced planarity caused by the interactions in the crystal packing could play a key role in the expansion of π-conjugation and the consequent narrowing of the HOMO–LUMO gap. In addition, we also carried out the calculations for the dimeric structure in the SC of the complexes (Tables S10 and S11). The calculated HOMO–LUMO gaps of the dimeric structures (E = 3.06 eV for **PhAlMe**; 2.85–2.88 eV for **PhGaMe**; 3.03 eV for **PhInMe**) were smaller than those of the single molecule in SC (E = 3.21 eV for **PhAlMe**; 3.27–3.32 eV for **PhGaMe**; 3.35 eV for **PhInMe**). These results suggest that the orbital interactions originating from the packing structures could affect the electronic transitions.

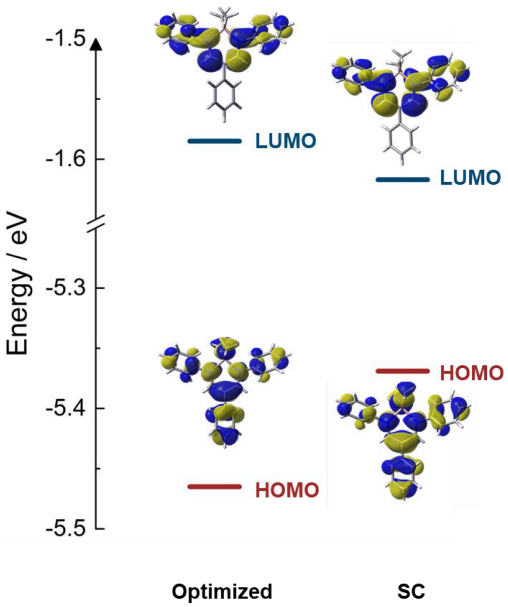

Figure 5. Molecular orbital diagrams of **PhAlMe** calculated at the level with PBE1PBE/6-31G(d,p). Single-point calculations were carried out for the DFT-optimized and single-crystal structures. SC denotes a single-crystal structure.

Table 7. Calculated parameters of the electronic transitions at the S_0 state for the DFT-optimized and single-crystal structures [a]

	Composition [b]	Coefficient [c]	E / eV	λ / nm	f [d]
Optimized	HOMO→LUMO	0.700	3.22	385	0.352
SC	HOMO→LUMO–1	–0.133	3.05	406	0.261
	HOMO→LUMO	0.694			

[a] Calculated at the level with PBE1PBE/6-31G(d,p). [b] Composition of the electronic states. [c] Coefficient for the electronic transition. [d] Oscillator strength.

Table 8. Selected dihedral angles in the DFT-optimized and single-crystal structures

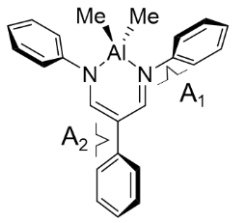

	Dihedral angle / °	
	A_1	A_2
Optimized	136	138
SCXRD	145	142

Conclusion

To evaluate the effects of the central elements on the photoluminescence properties of the complexes, we synthesized the series of the dialdiminate complexes involving group 13 elements with the same ligands. The ligand exchange reaction was observed in the solution of the indium complexes and monitored by ^{1}H NMR spectra and optical measurements. Controlling the reactions with the addition of $InCl_3$ and/or $InMe_3$ allowed us to modulate their optical properties. Comparing the photophysical properties of the aluminum, gallium, and indium complexes in their solution states, the difference in the absorption maxima was observed. The quantum calculations suggest that the difference should be derived from the difference in the partial charges on the central elements. In addition, the difference in the Lewis acidity between the three complexes was also observed from the evaluation of quantum yields in their solution states. The response to Lewis bases was also demonstrated by measuring their luminescent properties in some organic solvents with variable Lewis basicity. The aluminum complex exhibited dramatic changes in the photophysical properties depending on the Lewis bases, which might be ascribed to the more positively charged central element in comparison with the other complexes. Moreover, the AIEE and CIEE properties were observed from all complexes. Utilizing the dialdiminate backbone with excellent emission efficiencies in both solution

and solid states, this work offers a deeper insight into the effects of the differences in atomic properties on the optical properties of molecules. Our finding could be helpful for establishing a new strategy for electronically controlling the properties of the complexes by changing the central elements in the same group. In addition, the synthesized dialdiminate complexes have the potential for applications to film-type luminescent sensors for Lewis bases and to OLED by utilizing the good solubilities for any solvent, good film-forming abilities, and the Lewis base responsiveness unique to **PhAlMe**.

Experimental Section

Materials: All reactions were performed under nitrogen atmosphere using modified Schlenk line techniques and an MBRAUN glovebox system UNIlab. Analytical thin layer chromatography (TLC) was performed with silica gel 60 Merck F254 plates. Column chromatography was performed with Wakogel C-200 SiO_2. Phenylacetyl chloride (Tokyo Chemical Industry Co, Ltd.; TCI), aniline (Fujifilm Wako Pure Chemical Corporation; Wako), $POCl_3$ (TCI), $NaClO_4$ (Wako), trimethylaluminum (Kanto Chemical Co., Inc.; Kanto), anhydrous gallium trichloride (TCI), and methyllithium (Kanto) were purchased from the commercial sources and used as received. Anhydrous indium trichloride (Strem Chemicals, Inc.; Strem) was purified by sublimation method under inert atmosphere before use. Deoxygenated *N*,*N*-dimethylformamide (DMF; Wako), deoxygenated methanol (MeOH; Wako), deoxygenated hexane (Wako), deoxygenated toluene (Wako), deoxygenated acetonitrile (MeCN; Wako), deoxygenated tetrahydrofuran (THF; Wako), chloroform ($CHCl_3$; Wako), pyridine (Wako), dichloromethane (DCM; Wako), MeCN (Wako), anhydrous 2-methyltetrahydrofuran (2-MTHF; Sigma-Aldrich Co. LLC), and deuterated chloroform ($CDCl_3$; Cambridge Isotope Laboratories, Inc.; Eurisotop) were purchased from commercial sources and used as received. 2-Methylpentane (2-MP; TCI) was purified by fractional distillation in the presence of sodium/benzophenone under inert

atmosphere before use. Diethyl ether and triethylamine were purified using a two-column solid-state purification system (Glasscoutour System, Joerg Meyer, Irvine, CA). Deuterated dichloromethane (Eurisotop) was stored with microwave-activated molecular sieves 4A (Wako) and degassed in a glovebox before use.

Synthesis of 1: [16a] To DMF (25 mL) was added $POCl_3$ (18.1 mL, 29.8 g, 194 mmol) dropwise at room temperature under nitrogen. To the resulting reddish-brown solution was added phenylacetyl chloride (8.55 mL, 10.0 g, 64.7 mmol) and the mixture was stirred at 80 °C under nitrogen for 20 h. The reaction mixture was diluted with DMF and added dropwise to $NaClO_4$ aq. (0.24 M, 300 mL) at 0 °C. The precipitate was collected by suction filtration and washed with water and diethyl ether to give the product as a pale brown powder (14.6 g, 74%). ^{1}H NMR ($CDCl_3$, 400 MHz): δ 7.86 (s, 2H, N–C*H*=C), 7.42–7.38 (m, 3H, *Ar*), 7.29–7.27 (dd, 2H, J = 4.4 Hz, *Ar*), 3.35 (s, 6H, N–CH_3), 2.47 (s, 6H, N–CH_3) ppm. ^{13}C{^{1}H} NMR ($CDCl_3$, 100 MHz): δ 164.3, 132.4, 132.4, 129.3, 128.9, 106.0, 49.3, 39.7 ppm. HRMS (ESI) $[M]^+$: Found, 203.1541; Calcd., 203.1543.

Synthesis of 2: [18] To a solution of **1** (11.1 g, 36.8 mmol) in MeOH (190 mL) was added aniline (12.0 mL, 12.2 g, 131 mmol) and the mixture was stirred under reflux for 22 h.

The reaction mixture was evaporated with a rotary evaporator. The obtained solid was dissolved in a small amount of CH_2Cl_2, then poured into an excess amount of methanol at –78 °C. The precipitate was collected by suction filtration and dried under vacuum to afford a dark-yellow powder. The powder was purified by silica gel flash column chromatography with hexane/ethyl acetate (9/1) as an eluent. All volatiles were removed with a rotary evaporator. The obtained oil was dissolved in a small amount of CH_2Cl_2, then poured into an excess amount of hexane at –78 °C. The precipitant was collected by suction filtration and dried under vacuum to afford **2** as a yellow powder (3.87 g, 35%). ^{1}H NMR ($CDCl_3$, 400 MHz): δ 12.9 (s, 1H, N*H*), 8.07 (s, 2H, N–C*H*=C), 7.41–7.38 (m, 6H, *Ar*), 7.36 (dd, 2H, J = 7.2 Hz, *Ar*), 7.18–7.14 (m, 5H, *Ar*), 7.11 (t, 2H, J = 7.6 Hz, *Ar*) ppm. ^{13}C{^{1}H} NMR ($CDCl_3$, 100 MHz): δ 149.4, 146.6, 140.4, 129.6, 128.9, 126.2, 125.7, 124.0, 118.5, 109.7 ppm. HRMS (ESI) $[M+H]^+$: Found, 299.1543; Calcd., 299.1543.

Synthesis of PhAlMe: To a solution of **2** (0.50 g, 1.7 mmol) in toluene (17 mL) was added $AlMe_3$ (1.06 M in hexane, 1.9 mL, 2.0 mmol) dropwise at 0 °C under nitrogen and the reaction mixture was stirred at room temperature for 18 h. The solution was evaporated with a rotary evaporator. The obtained oil was dissolved in toluene and filtered. The filtrate was evaporated with a rotary evaporator and the obtained oil was dissolved

in hexane. The solution was slowly evaporated to afford **PhAlMe** as a yellow crystal (60 mg, 10%). ^{1}H NMR (CD_2Cl_2, 400 MHz): δ = 7.94 (s, 2H, N–C*H*=C), 7.40 (dd, 4H, J = 8.0 Hz, *Ar*), 7.35 (d, 2H, J = 4.4 Hz, *Ar*), 7.27–7.21 (m, 7H, *Ar*), –0.72 (s, 6H, Al–CH_3) ppm. ^{13}C{^{1}H} NMR (CD_2Cl_2, 100 MHz): δ 160.0, 148.6, 140.0, 129.5, 128.8, 125.9, 125.7, 125.5, 122.5, 109.8, –8.77 ppm. HRMS (ESI) $[M+H]^+$: Found, 397.1196; Calcd., 397.1190. Anal. Calcd. for $C_{23}H_{23}AlN_2$: C, 77.94; H, 6.54; Al, 7.62; N, 7.90%. Found: C, 78.03; H, 6.52; Al, 7.56; N, 7.89%.

Synthesis of PhGaCl: Anhydrous gallium trichloride (0.71 g, 4.0 mmol) was dissolved in diethyl ether (15 mL) and stirred at 0 °C under nitrogen. The solution was added to a solution of **2** (0.30 g, 1.0 mmol) in toluene (23 mL). To the mixture solution was added triethylamine (0.56 mL, 0.41 g, 4.0 mmol) and stirred at 100 °C for 20 h. The reaction mixture was evaporated with a rotary evaporator. The obtained oil was dissolved in a small amount of CH_2Cl_2, then poured into an excess amount of MeOH at –78 °C. The precipitate was collected by suction filtration and dried under vacuum to afford **PhGaCl** as a yellow powder (0.40 g, 91%). ^{1}H NMR ($CDCl_3$, 400 MHz): δ 8.05 (s, 2H, N–C*H*=C), 7.50–7.43 (m, 8H, *Ar*), 7.42–7.30 (m, 7H, *Ar*) ppm. ^{13}C{^{1}H} NMR ($CDCl_3$, 100 MHz): δ 160.4, 146.2, 138.5, 129.9, 129.1, 127.2, 126.8, 126.7, 122.6, 110.2 ppm. HRMS (ESI)

[M+Cl]$^-$: Found, 470.9717; Calcd., 470.9719. Anal. Calcd. for $C_{21}H_{17}Cl_2GaN_2$: C, 57.59; H, 3.91; Cl, 16.19; Ga, 15.91; N, 6.40%. Found: C, 57.41; H, 3.92; Cl, 16.14; Ga, 16.15; N, 6.38%.

Synthesis of PhGaMe: To a solution of **PhGaCl** (50 mg, 0.11 mmol) in toluene (1.2 mL) was added methyllithium (1.12 M in diethyl ether, 0.25 mL, 0.28 mmol) dropwise at –78 °C under nitrogen and the reaction mixture was stirred at room temperature for 17 h. The solution was filtered and washed with toluene. The filtrate was evaporated with a rotary evaporator. The obtained oil was dissolved in a small amount of CH_2Cl_2, then poured into an excess amount of MeOH at –78 °C. The precipitate was collected by suction filtration and washed with cooled MeOH to afford **PhGaMe** as an orange powder (5.4 mg, 12%). ^{1}H NMR (CD_2Cl_2, 400 MHz): δ = 7.86 (s, 2H, N–C*H*=C), 7.37 (dd, 4H, J = 8.4 Hz, *Ar*), 7.35–7.32 (m, 4H, *Ar*), 7.21 (dd, 1H, J = 4.8 Hz, *Ar*), 7.19 (d, 4H, J = 4.0 Hz, *Ar*), 7.17 (dd, 2H, J = 5.6 Hz, *Ar*), –0.25 (s, 6H, Ga–CH_3) ppm. ^{13}C{^{1}H} NMR (CD_2Cl_2, 100 MHz): δ 158.4, 149.8, 141.4, 129.8, 129.1, 126.3, 125.6, 122.3, 109.3, –5.94 ppm. HRMS (ESI) [M+H]$^+$: Found, 397.1196; Calcd., 397.1190. Anal. Calcd. for $C_{23}H_{23}GaN_2$: C, 69.55; H, 5.84; Ga, 17.56; N, 7.05%. Found: C, 69.72; H, 5.78; Ga, 17.47; N, 7.03%.

Synthesis of PhInMe: To a solution of $InCl_3$ (0.39 g, 1.8 mmol) in Et_2O (18 mL) was added methyllithium (1.12 M in diethyl ether, 4.7 mL, 5.3 mmol) dropwise at –78 °C under nitrogen and the reaction mixture was stirred at room temperature for 30 min. To the white suspension was added a solution of **2** (0.50 g, 1.7 mmol) in toluene (17 mL) at –78 °C under nitrogen and the reaction mixture was stirred at room temperature for 1 h. After the solvent was removed in vacuum, the obtained yellow oil was dissolved in toluene and filtered with a PTFE syringe filter (0.20 μm). The filtrate was concentrated in vacuum and the obtained oil was dissolved in hexane. The solution was slowly evaporated to afford the products as an orange crystal (0.17 mg, 23%). Although the expected structure of **PhInMe** was fully characterized by SCXRD, the NMR and HRMS spectra of its solutions indicated the existence of **PhInMeCl** as a minor species (19 mol% in CD_2Cl_2). We concluded that the chlorinated species would be generated by the equilibrium reactions with a trace amount of unremovable byproducts such as $InMe_nCl_{(3-n)}$ (n = 1–3) in the solution states. Therefore, the following characterization data were provided for both compounds. For **PhInMe**: ^{1}H NMR (CD_2Cl_2, 800 MHz): δ = 7.84 (s, 2H, N–C*H*=C), 7.34–7.32 (m, 9H, *Ar*), 7.30 (d, 2H, J = 5.6 Hz, *Ar*), 7.28 (t, 1H, J = 7.2 Hz, *Ar*), 7.18 (dd, 2H, J = 7.2 Hz, *Ar*), 7.17 (t, 2H, J = 8.0 Hz, *Ar*), 7.08 (d, 2H, J = 6.4

Hz, *Ar*), –0.15 (s, 6H, In–CH_3) ppm. $^{13}C\{^1H\}$ NMR (CD_2Cl_2, 200 MHz): δ 159.9, 151.2, 142.6, 129.6, 128.5, 126.4, 124.8, 124.5, 121.1, 108.9, –7.34 ppm. HRMS (DART) $[M+H]^+$: Found, 443.0969; Calcd., 443.0973. For **PhInMeCl**: ^1H NMR (CD_2Cl_2, 800 MHz): δ = 8.00 (s, 2H, N–C*H*=C), 7.40 (dd, 4H, J = 4.8 Hz, *Ar*), 7.34–7.32 (m, 9H, *Ar*), 7.31 (d, 4H, J = 7.2 Hz, *Ar*), 7.26 (t, 2H, J = 7.2 Hz, *Ar*), 0.23 (s, 6H, In–CH_3) ppm. $^{13}C\{^1H\}$ NMR (CD_2Cl_2, 200 MHz): δ 160.4, 149.7, 141.2, 130.0, 128.7, 127.0, 125.8, 125.7, 121.4, 109.6, –8.29 ppm. HRMS (DART) $[M+H]^+$: Found, 463.0420; Calcd., 463.0432.

NMR Spectra: ^1H and $^{13}C\{^1H\}$ NMR spectra were recorded on JEOL JNM-AL400 (at 400 and 100 MHz, respectively), JNM-ECZ400 (at 400 and 100 MHz, respectively) or Bruker AVANCE III 800US PLUS (at 800 and 200 MHz, respectively) spectrometers. Bruker AVANCE III 800US PLUS spectroscopy was utilized in the measurements for the mixture solution of **PhInMe** and **PhInMeCl**. In ^1H and $^{13}C\{^1H\}$ NMR spectra, tetramethylsilane (TMS) and/or residual solvents were used as an internal standard.

Optical Property Measurements: UV−vis absorption spectra were recorded on a SHIMADZU UV3600i Plus spectrophotometer. Fluorescence, phosphorescence, and

excitation spectra were measured with a HORIBA JOBIN YVON Fluorolog–3 spectrofluorometer. Photoluminescence (PL) lifetimes were measured with a Horiba FluoroCube spectrofluorometer system and excitation was carried out at 369 nm using a UV diode laser (NanoLED 369 nm). The cryogenic measurements in PL spectra and lifetimes were performed by Oxford Optistat DN2. PL quantum yields were measured with Hamamatsu Photonics Quantaurus-QY Plus C13534-01 model and calculated by integrating sphere method. The cryogenic measurements for PL quantum yields were carried out with a Dewar flask as a sample holder.

Mass Spectrometry: High-resolution mass spectra (HRMS) were measured on a Thermo Fisher Scientific EXACTIVE for electron spray ionization (ESI) and direct analysis in real time (DART) at the Technical Support Office (Department of Synthetic Chemistry and Biological Chemistry, Graduate School of Engineering, Kyoto University). The HRMS with the method of DART was carried out in the characterization of the byproducts in the crystal and solution of **PhInMe**.

Elemental Analysis: Elemental analysis was performed at the Microanalytical Center of Kyoto University.

X-ray Diffraction Measurements: Powder X-ray diffraction (PXRD) patterns were taken by using CuKα radiation with Rigaku SmartLab. Single-crystal X-ray diffraction (SCXRD) patterns were measured by using MoKα radiation with Rigaku Varimax at 150 K.

Deposition Number(s) <url href="https://www.ccdc.cam.ac.uk/services/structures?id=doi:10.1002/###.202200654" > 2245207 (for **PhAlMe**), 2245210 (for **PhGaMe**), 2245211 (for **PhInMe**)</url> contain(s) the supplementary crystallographic data for this paper. These data are provided free of charge by the joint Cambridge Crystallographic Data Centre and Fachinformationszentrum Karlsruhe <url href="http://www.ccdc.cam.ac.uk/structures">Access Structures service</url>.

Supporting Information

Additional references cited within the Supporting Information.[19]

Acknowledgements

A part of computation time was provided by the SuperComputer System, Institute for Chemical Research, Kyoto University. This work was partially supported by a Grant-in-Aid for Early-Career Scientists (for S.I., JSPS KAKENHI Grant Numbers 21K14673), for Scientific Research (B) (for K.T., JSPS KAKENHI Grant Number, 21H02001), and for Exploratory Research (for K.T., JSPS KAKENHI Grant numbers 21K19002).

Conflicts of Interest

The authors declare no conflicts of interest.

Keywords

aluminum, gallium, group 13 elements, heterocycles, indium, luminescence

References

[1] (a) D. Frath, J. Massue, G. Ulrich, R. Ziessel, *Angew. Chem. Int. Ed*. **2014**, *53*, 2290–2310. (b) D. Li, H. Zhang, Y. Wang, *Chem. Soc. Rev*., **2013**, *42*, 8416. (c) Y. Adachi, Y. Ooyama, Y. Ren, X. Yin, F. Jäkle, J. Ohshita, *Polym. Chem*., **2018**, *9*, 291–299.

[2] (a) W. Zhou, N. Yutronkie, B. Lessard, J. Brusso, *Mater. Adv.* **2021**, *2*, 165. (b) Y. Min, C. Dou, H. Tian, Y. Geng, J. Liu, L. Wang, *Angew. Chem. Int. Ed*. **2018**, *57*, 2000–2004.

[3] (a) P. Su, L. Wen, Y. Zhou, J. Yan, X. Yuan, D. Liu, K. Zheng, N. Zhang, *Chem. Eur. J*. **2022**, *28*, e2022013. (b) X. Cheng, D. Li, Z. Zhang, H. Zhang, Y. Wang, *Org. Lett.* **2014**, *16*, 880–883. (c) M. Gon, K. Tanaka, Y. Chujo, *Angew. Chem. Int. Ed*. **2018**, *57*, 6546–6551.

[4] A. Sumiyoshi, Y. Chiba, R. Matsuoka, T. Noda, T. Nabeshima, *Dalton Trans*. **2019**, *48*, 13169–13175.

[5] (a) S. Yamaguchi, S. Akiyama, K. Tamao, *J. Am. Chem. Soc*. **2001**, *123*, 11372–11375. (b) N. Kameta, K. Hiratani, *Chem. Lett*. **2006**, *35*, 536. (c) A. Oehlke, A. A. Auer, K. Schreiter, N. Friebe, S. Spange, *Chem. Eur. J.* **2015**, *21*, 17890–17896.

[6] (a) Q. Hou, L. Liu, S. K. Mellerup, N. Wang, T. Peng, P. Chen, S. Wang, *Org. Lett.* **2018**, *20*, 6467–6470. (b) Y. G. Shi, J. W. Wang, H. Li, G. F. Hu, X. Li, S. K. Mellerup, N. Wang, T. Peng, S. Wang, *Chem. Sci*., **2018**, *9*, 1902–1911.

[7] K. Matsuo, S. Saito, S. Yamaguchi, *J. Am. Chem. Soc*. **2014**, *136*, 36, 12580–12583.

[8] (a) S. Oda, W. Kumano, T. Hama, R. Kawasumi, K. Yoshiura, T. Hatakeyama, *Angew. Chem. Int. Ed.* **2021**, *60*, 2882–2886. (b) Y. Shiu, Y. Cheng, W. Tsai, C. Wu, C. Chao, C. Lu, Y. Chi, Y. Chen, S. Liu, P. Chou, *Angew. Chem. Int. Ed*. **2016**, *55*, 3017–3021.

[9] (a) L. Wang, X. Jiang, Z. Zhang, S. Xu, *Displays* **2000,** *21*, 47–49. (b) F. F. Muhammad, K. Sulaiman, *Measurement* **2011**, *44*, 1468–1474.

[10] H. A. Baalbaki, K. Nyamayaro, J. Shu, C. Goonesinghe, H. J. Jung, P. Mehrkhodavandi, *Inorg. Chem*. **2021**, *60*, 19304–19314.

[11] (a) T. Matsumoto, K. Tanaka, Y. Chujo, *J. Am. Chem. Soc*. **2013**, *135*, 4211–4214. (b) T. Matsumoto, K. Tanaka, K. Tanaka, Y. Chujo, *Dalton Trans*., **2015**, *44*, 8697–8707. (c) R. Inaba, K. Oka, T. Iwami, Y. Miyake, K. Tajima, H. Imoto, K. Naka, *Inorg. Chem*. **2022**, *61*, 7318−7326.

[12] W. Schorn, D. Grosse-Hagenbrock, B. Oelkers, J. Sundermeyer, *Dalton Trans*.,**2016**, *45*,1201–1207.

[13] (a) C. G. Gianopoulos, N. Kumarr, Y. Zhao, L. Jia, K. Kirschbaum, M. R. Mason, *Dalton Trans.*, **2016**, *45*, 13787–13797. (b) W. Wan, M. S. Silva, C. D. McMillen, S. E. Creager, R. C. Smith, *J. Am. Chem. Soc*. **2019**, *141*, 8703–8707.

[14] (a) S. Singh, H. Ahn, A. Stasch, V. Jancik, H. W. Roesky, A. Pal, M. Biadene, R. Herbst-Irmer, M. Noltemeyer, H. Schmidt, *Inorg. Chem*. **2006**, *45*, 1853–1860. (b) R. L. Webster, *Dalton Trans*. **2017**, *46*, 4483–4498.

[15] (a) M. Stender, B.E. Eichler, N. J. Hardman, P. P. Power, J. Prust, M. Noltemeyer, H. W. Roesky, *Inorg. Chem*. **2001**, *40*, 2794–2799. (b) R. Yoshii, A. Hirose, K. Tanaka, Y. Chujo, *Chem. Eur. J*. **2014**, *20*, 8320–8324. (c) M. Yamaguchi, S. Ito, A. Hirose, K. Tanaka, Y. Chujo, *J. Mater. Chem. C* **2016**, *4*, 5314. (d) S. Ito, A. Hirose, M. Yamaguchi, K. Tanaka, Y. Chujo, *J. Mater. Chem. C* **2016**, *4*, 5564–5571. (e) S. Ito, A. Hirose, M. Yamaguchi, K. Tanaka, Y. Chujo, *Polymers* **2017**, *9*, 68. (f) R. Yoshii, A. Hirose, K. Tanaka, Y. Chujo, *J. Am. Chem. Soc*. **2014**, *136*, 18131–18139.

[16] (a) I. Davies, J. Marcoux, J. Wu, M. Palucki, E. Corley, M. Robbins, N. Tsou, R. Ball, P. Dormer, R. Larsen, P. Reider, J. Org. Chem. 2000, 65, 4571–4574. (b)

[17] Gaussian 16, Revision C.01, M. J. Frisch, G. W. Trucks, H. B. Schlegel, G. E. Scuseria, M. A. Robb, J. R. Cheeseman, G. Scalmani, V. Barone, G. A. Petersson, H. Nakatsuji, X. Li, M. Caricato, A. V. Marenich, J. Bloino, B. G. Janesko, R. Gomperts,

B. Mennucci, H. P. Hratchian, J. V. Ortiz, A. F. Izmaylov, J. L. Sonnenberg, D. Williams-Young, F. Ding, F. Lipparini, F. Egidi, J. Goings, B. Peng, A. Petrone, T. Henderson, D. Ranasinghe, V. G. Zakrzewski, J. Gao, N. Rega, G. Zheng, W. Liang, M. Hada, M. Ehara, K. Toyota, R. Fukuda, J. Hasegawa, M. Ishida, T. Nakajima, Y. Honda, O. Kitao, H. Nakai, T. Vreven, K. Throssell, J. A., Jr. Montgomery, J. E. Peralta, F. Ogliaro, M. J. Bearpark, J. J. Heyd, E. N. Brothers, K. N. Kudin, V. N. Staroverov, T. A. Keith, R. Kobayashi, J. Normand, K. Raghavachari, A. P. Rendell, J. C. Burant, S. S. Iyengar, J. Tomasi, M. Cossi, J. M. Millam, M. Klene, C. Adamo, R. Cammi, J. W. Ochterski, R. L. Martin, K. Morokuma, O. Farkas, J. B. Foresman, D. J. Fox, Gaussian, Inc, Wallingford, CT **2016**.

[18] R. Gompper, T. Müller, K. Polborn, *J. Mater. Chem*. **1998**, *8*, 2011–2018.

[19] (a) Lippert, E. Z. *Naturforsch. A* **1955**, *10*, 541–545. (b) N. Mataga, Y. Kaifu, M. Koizumi, *Bull. Chem. Soc. J*. **1956**, *29*, 465–470.

TOC Graphic

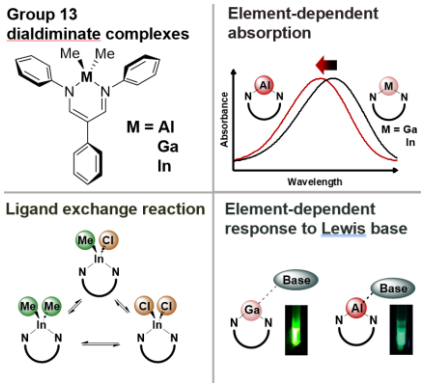

TOC Text

Element-dependent photophysical properties were observed from dialdiminate complexes containing group 13 elements. Alteration of the central elements results in the shift in the absorption wavelength and the enhancement of responsiveness toward Lewis bases, and the appearance of the ligand exchange reactions. In this paper, the mechanisms are explored.

Twitter: @univkyoto

NMR Spectra

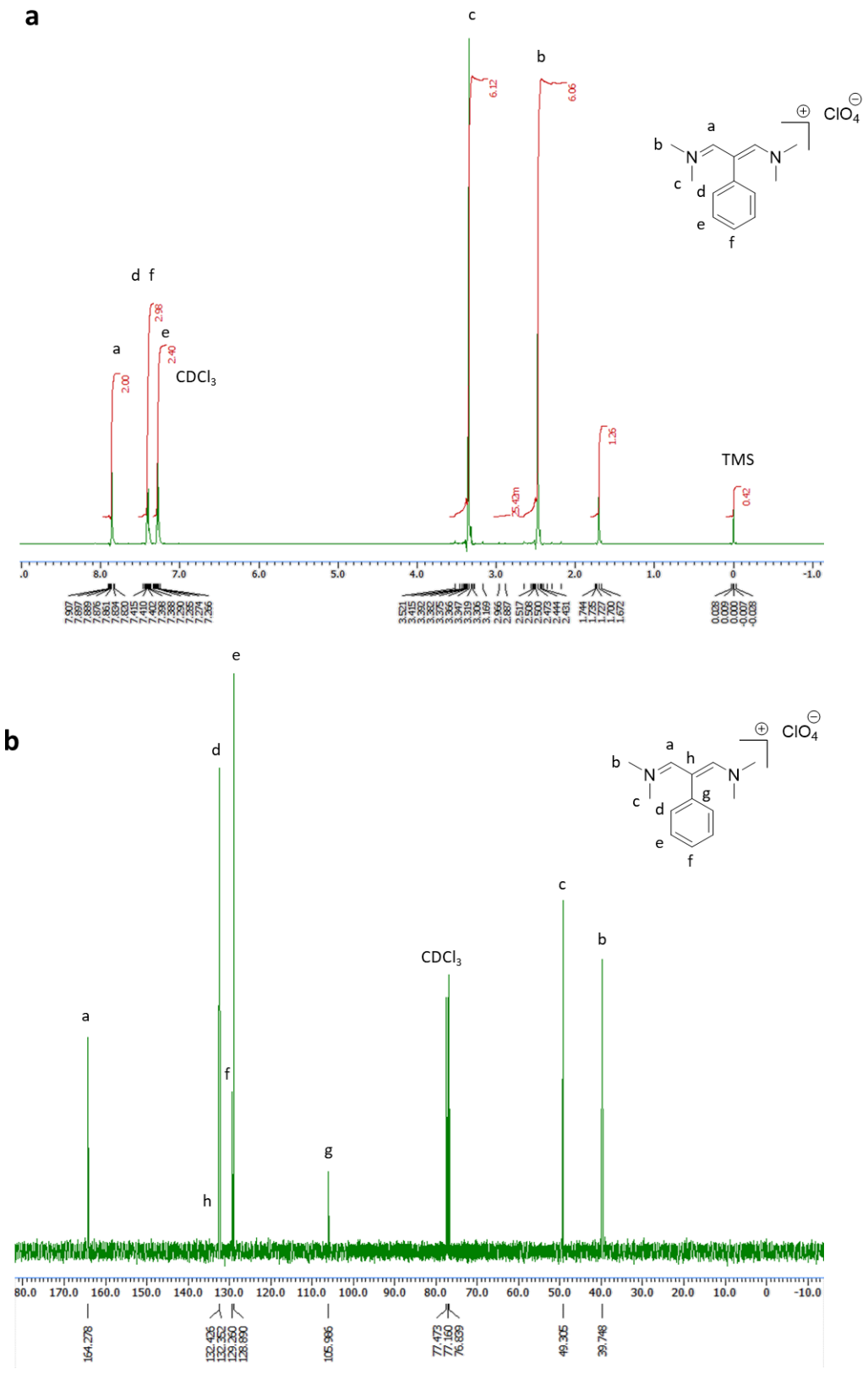

Figure S1. (a) ^{1}H and (b) ^{13}C NMR spectra of **1** in $CDCl_3$.

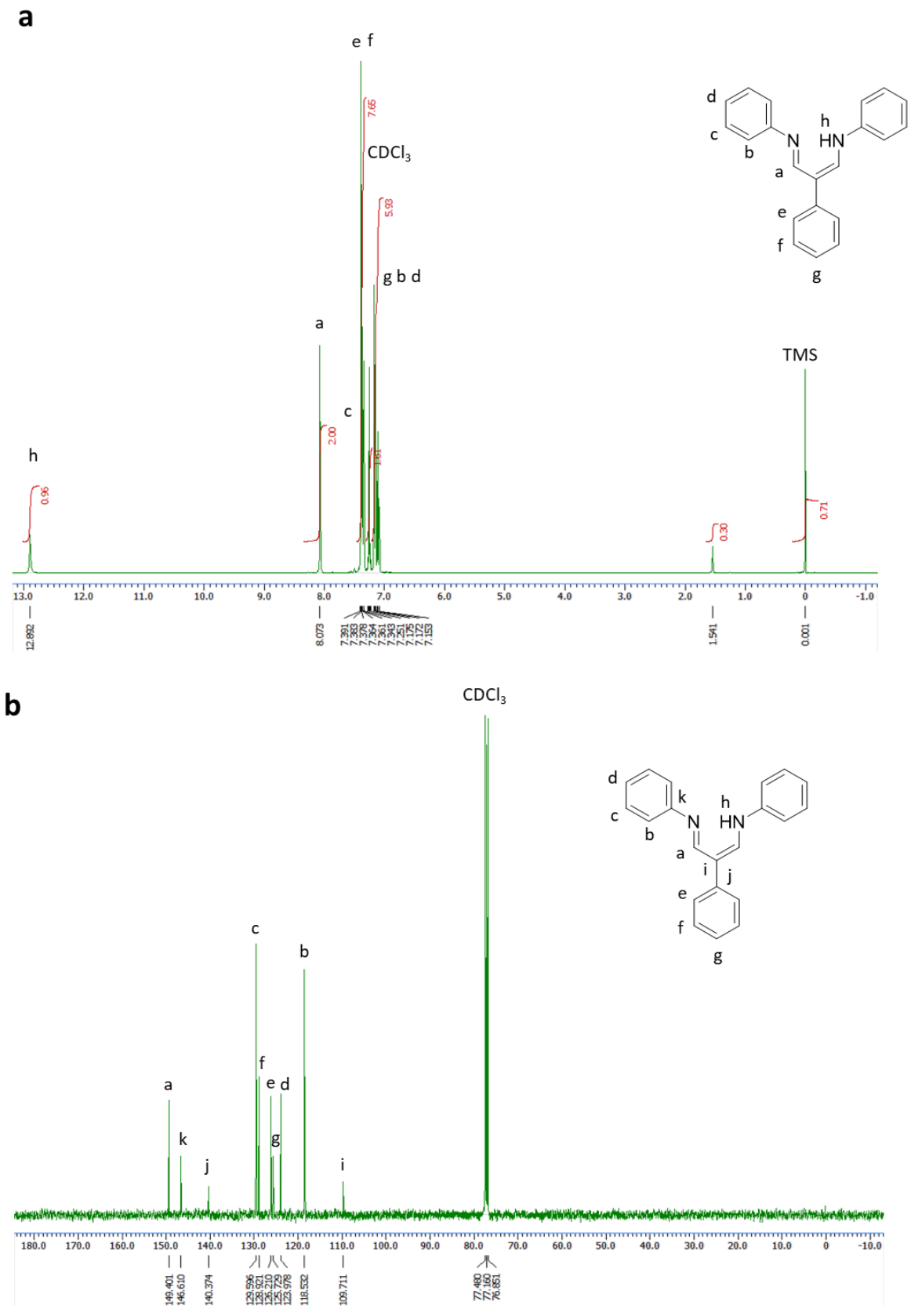

Figure S2. (a) ^{1}H and (b) ^{13}C NMR spectrum of **2** in $CDCl_3$.

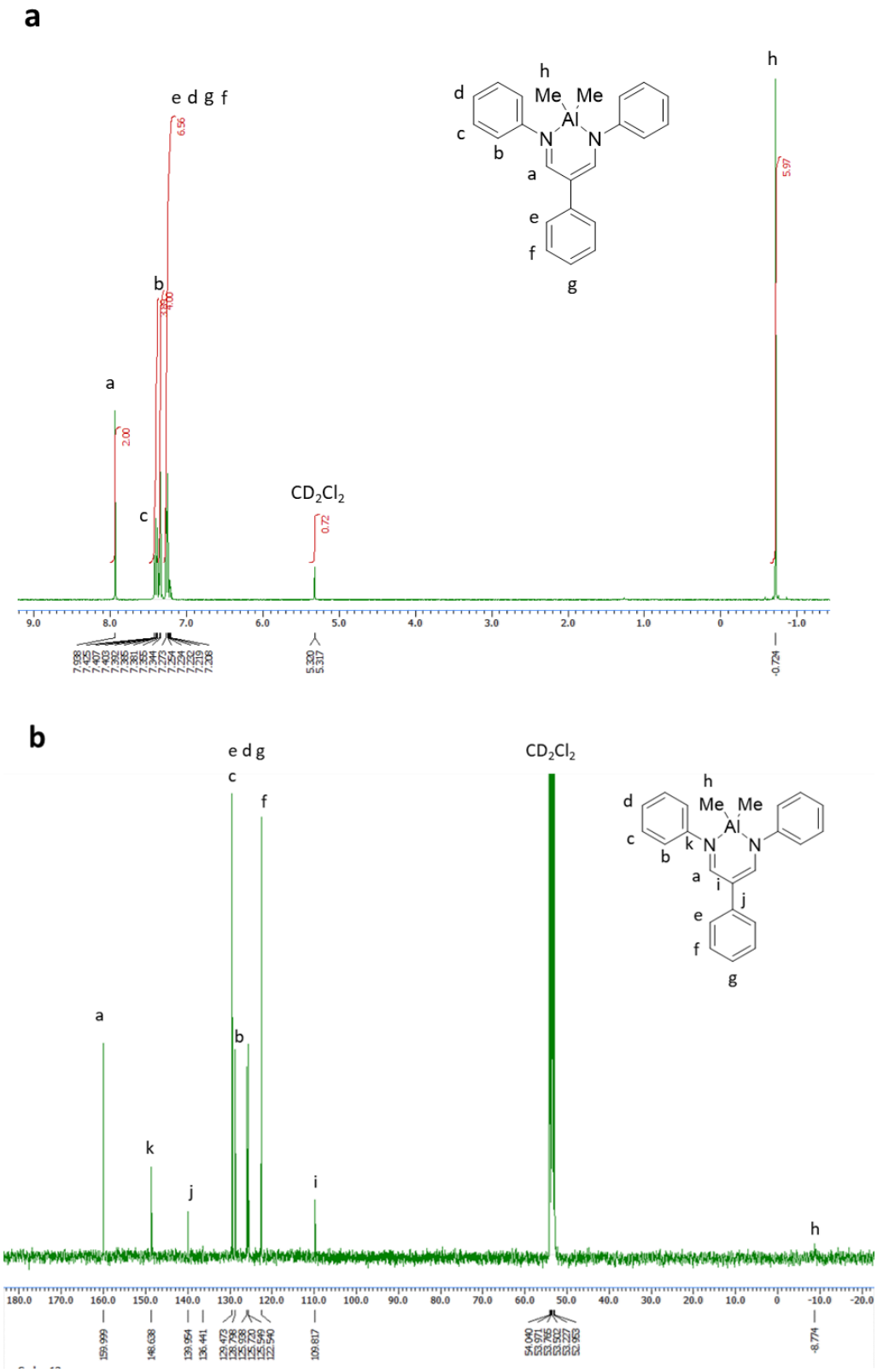

Figure S3. (a) ^{1}H and (b) ^{13}C NMR spectrum of **PhAlMe** in CD_2Cl_2.

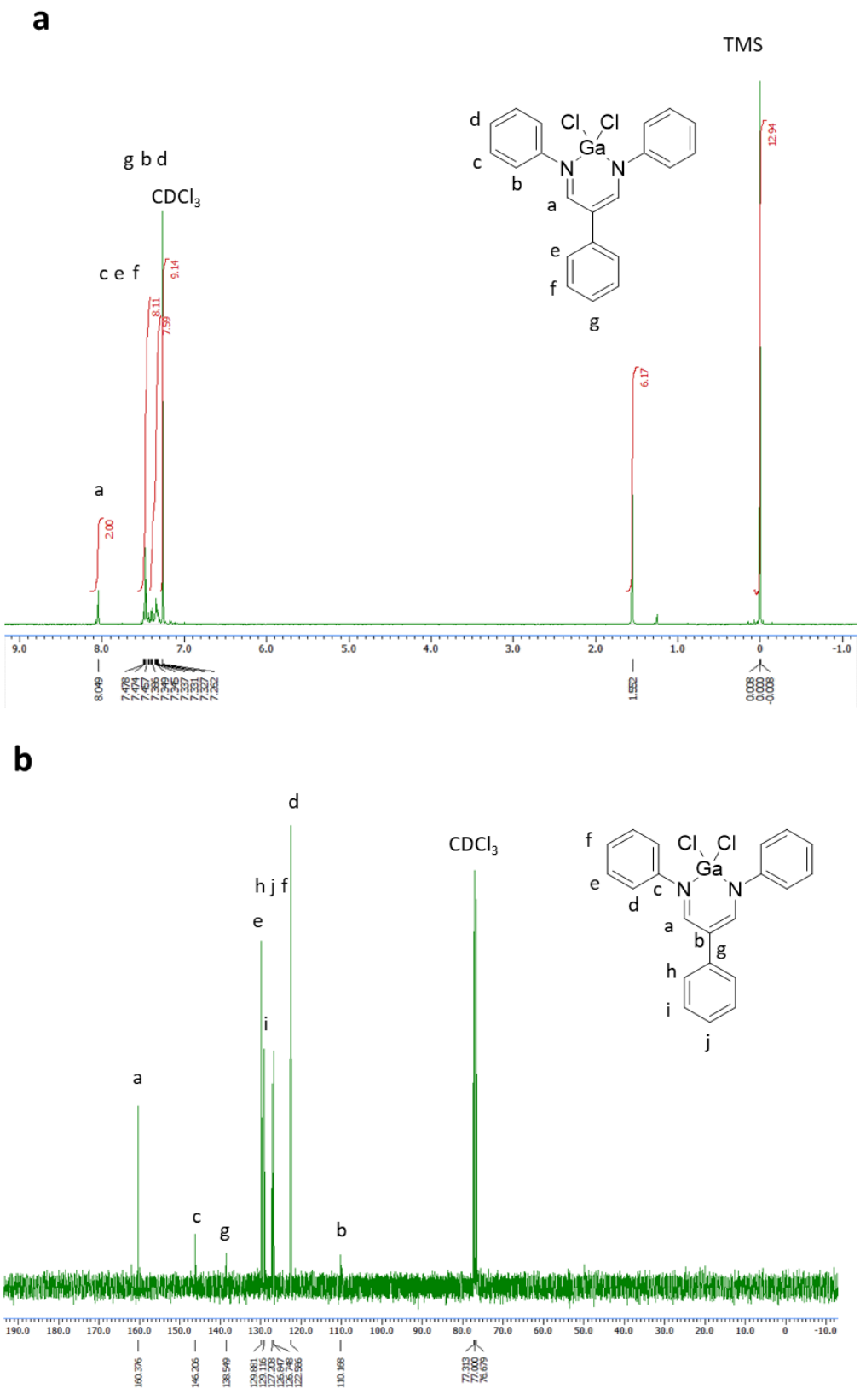

Figure S4. (a) ^{1}H and (b) ^{13}C NMR spectrum of **PhGaCl** in $CDCl_3$.

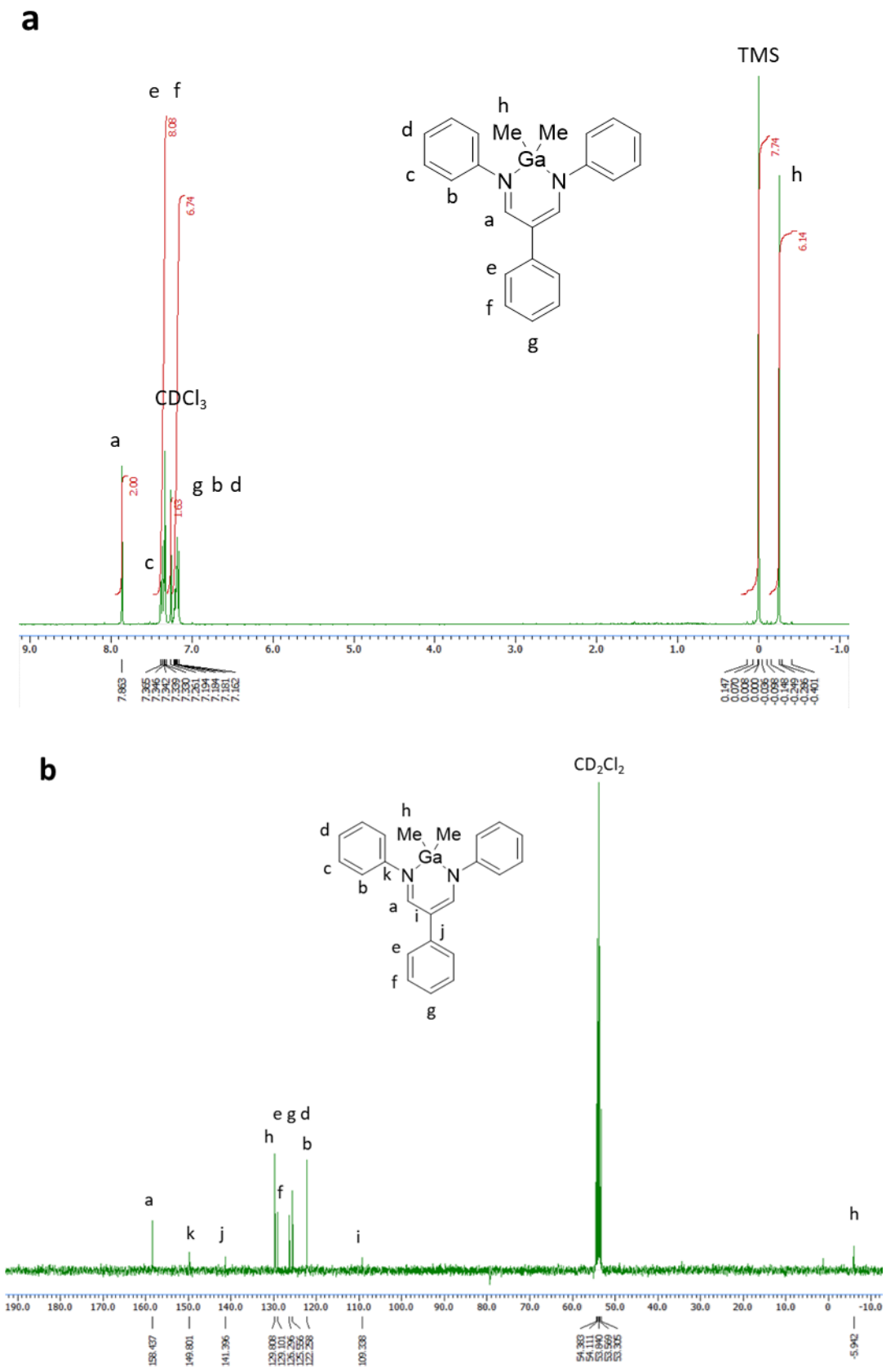

Figure S5. (a) ^{1}H and (b) ^{13}C NMR spectrum of **PhGaMe** in CD_2Cl_2.

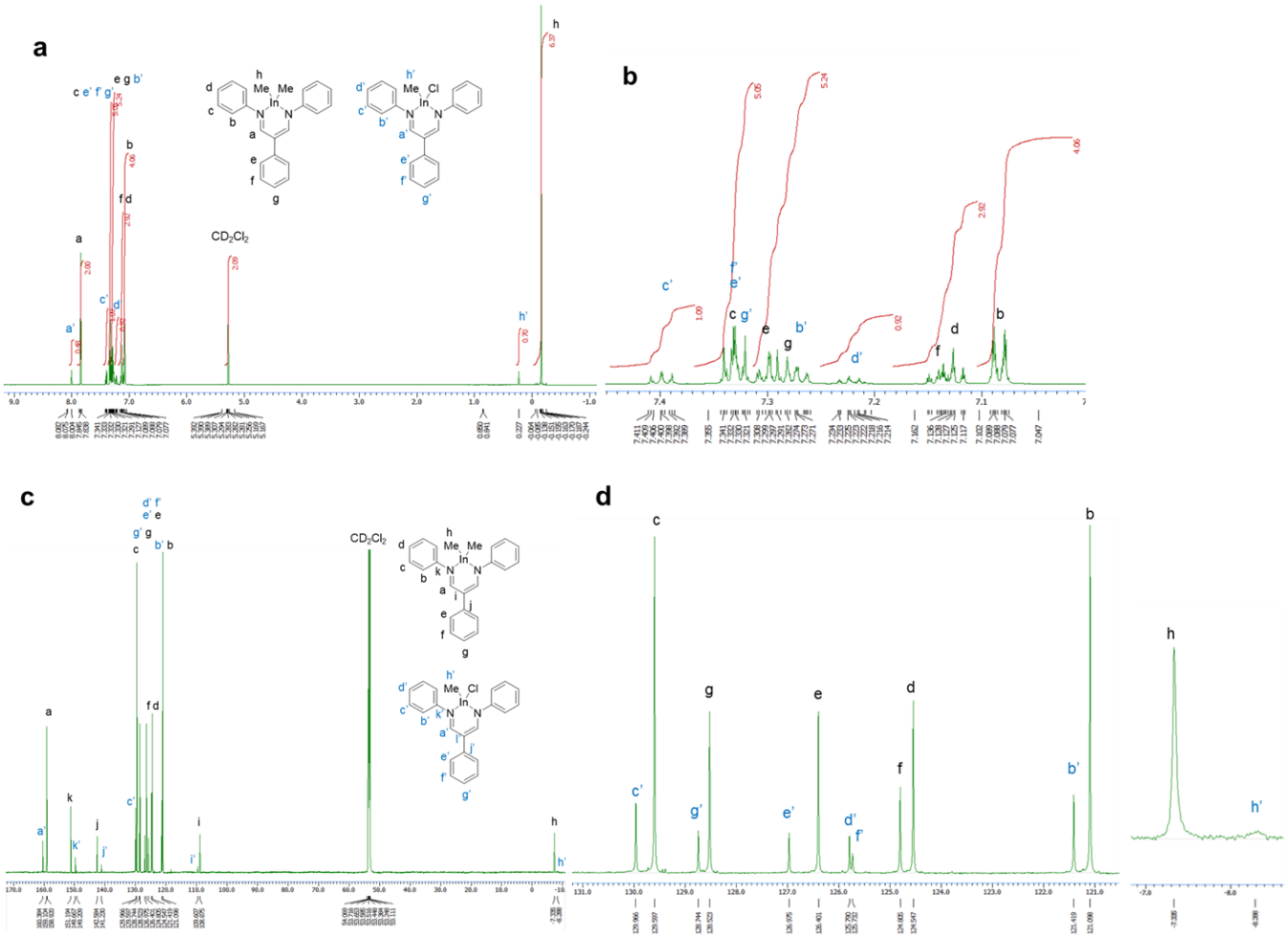

Figure S6. (a) ^{1}H and (c) ^{13}C NMR spectra of crystallographically pure **PhInMe** in CD_2Cl_2, which is in the equilibrium with **PhInMeCl**. Enlarged views of (b) ^{1}H and (d) ^{13}C NMR spectra, respectively.

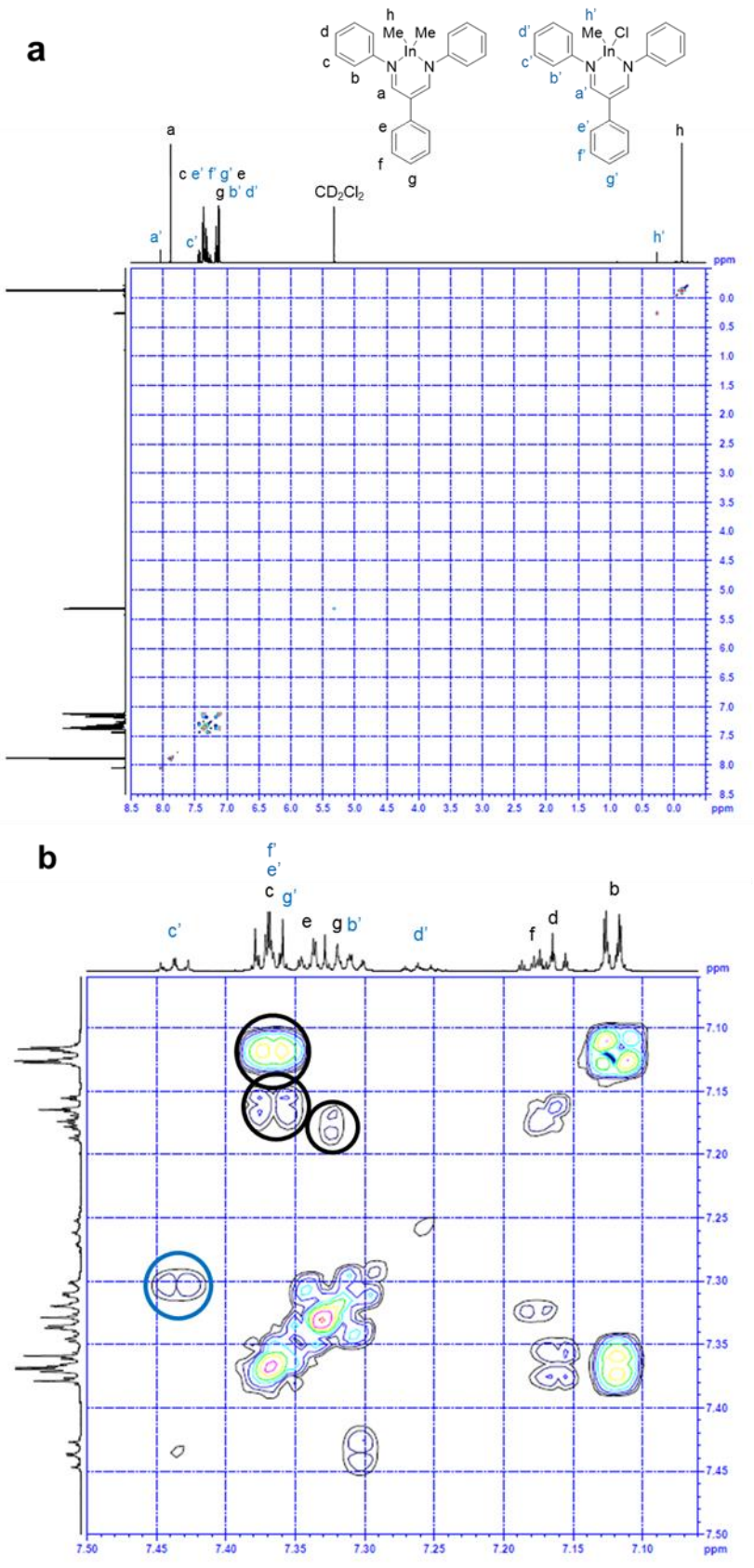

Figure S7. (a) ^{1}H–^{1}H COSY spectrum of crystallographically pure **PhInMe** in CD_2Cl_2 and (b) its enlarged view.

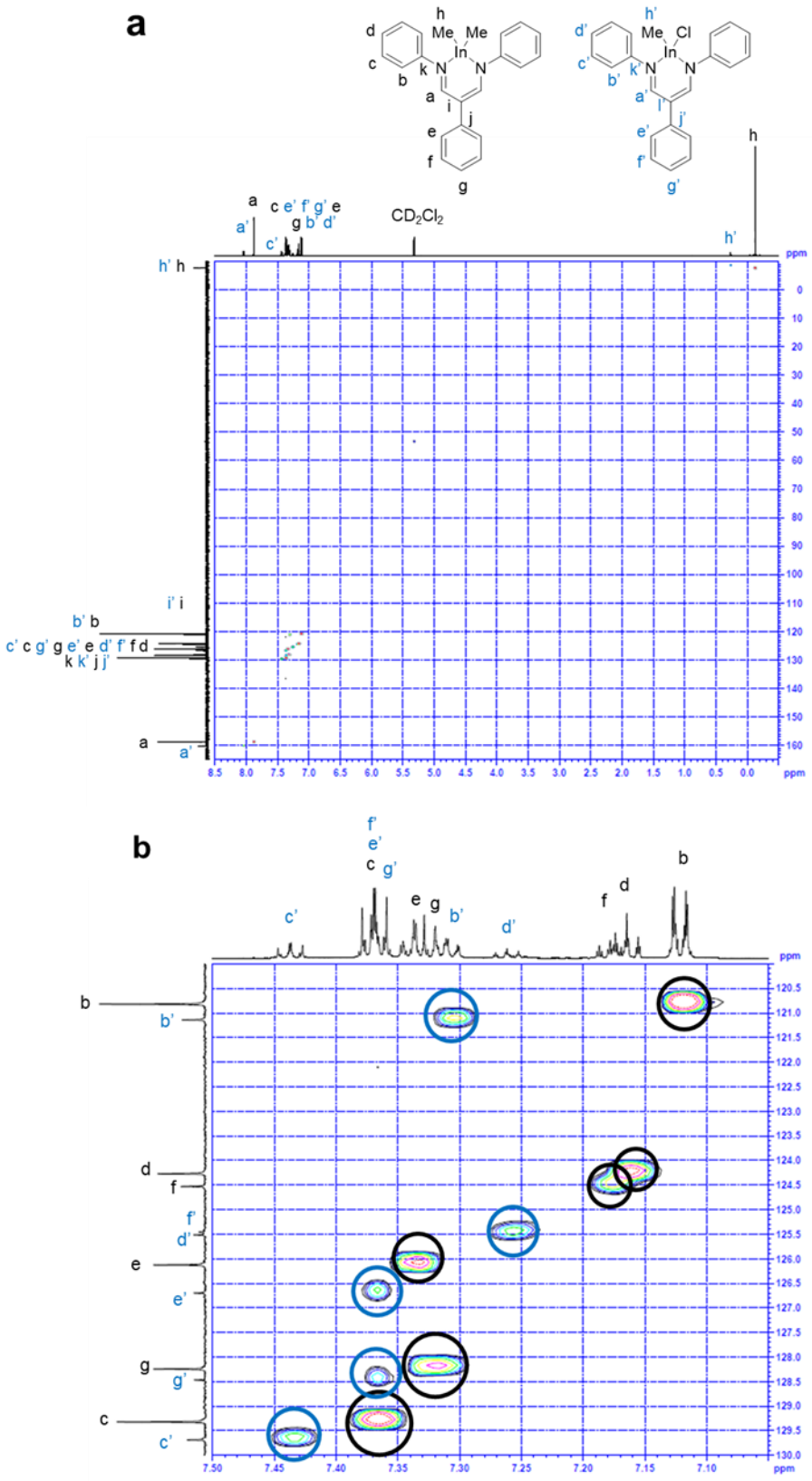

Figure S8. (a) $^{1}H–^{13}C$ HSQC spectrum of crystallographically pure **PhInMe** in CD_2Cl_2 (b) and its enlarged view.

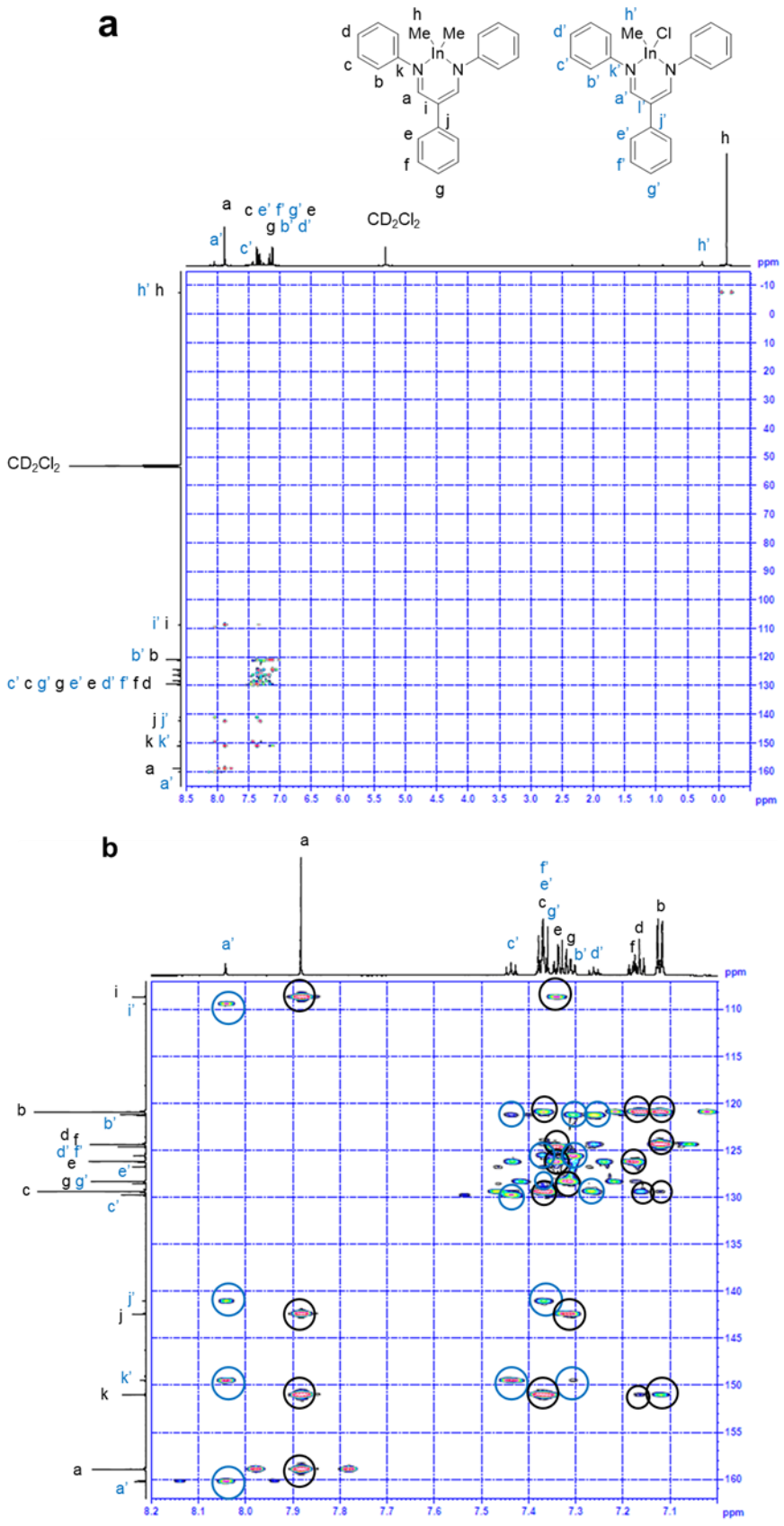

Figure S9. (a) $^{1}H–^{13}C$ HMBC spectrum of crystallographically pure **PhInMe** in CD_2Cl_2 and (b) its enlarged view.

Optical Property Measurements

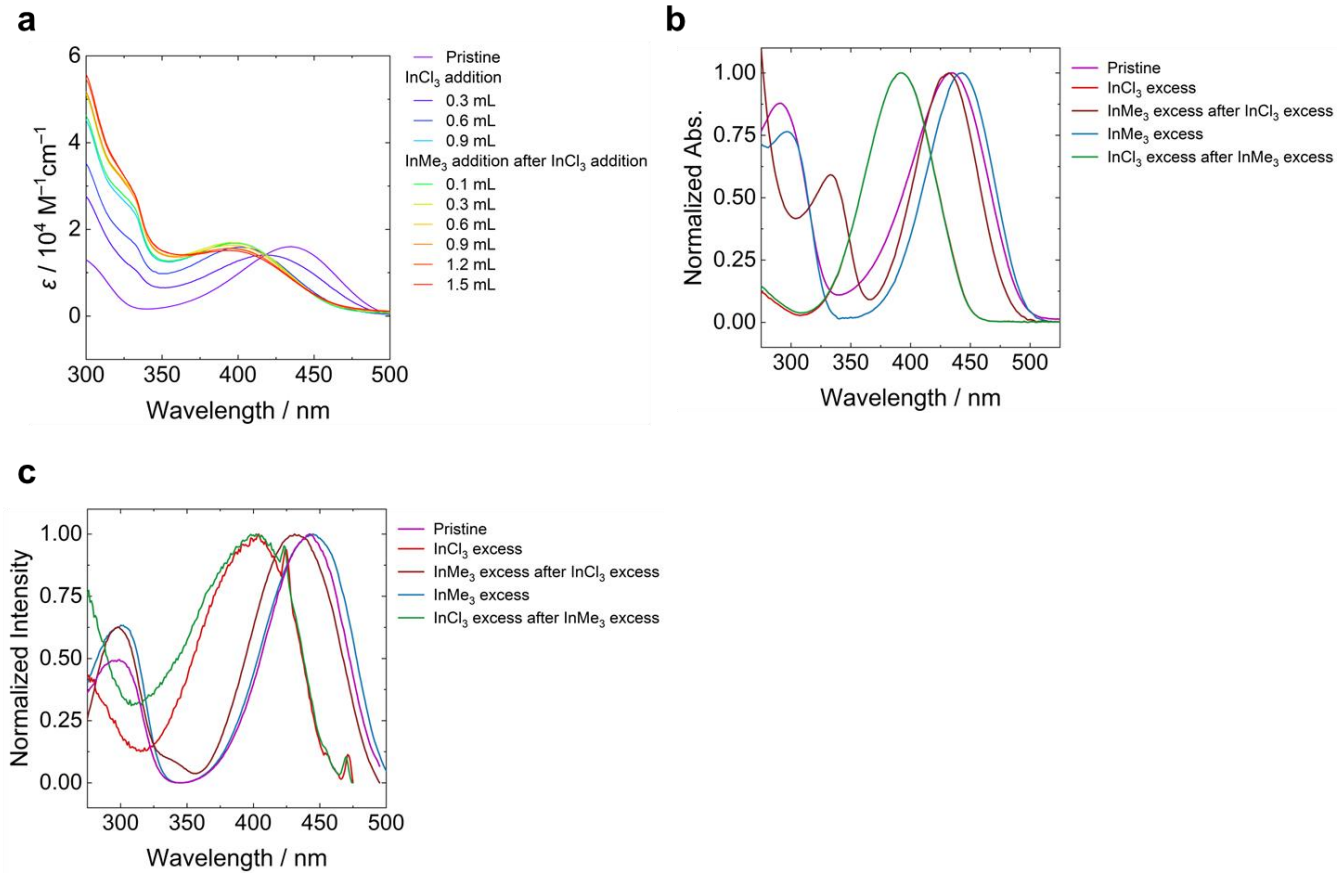

Figure S10. (a) Changes in absorption spectra of a 1.0×10^{-5} M solution of **PhInMe** with the subsequent addition of the saturated $InCl_3$ and $InMe_3$ solutions in CH_2Cl_2. Changes in (b) absorption and (c) excitation spectra of a 1.0×10^{-5} M solution of **PhInMe** with the additions of $InCl_3$ and/or $InMe_3$.

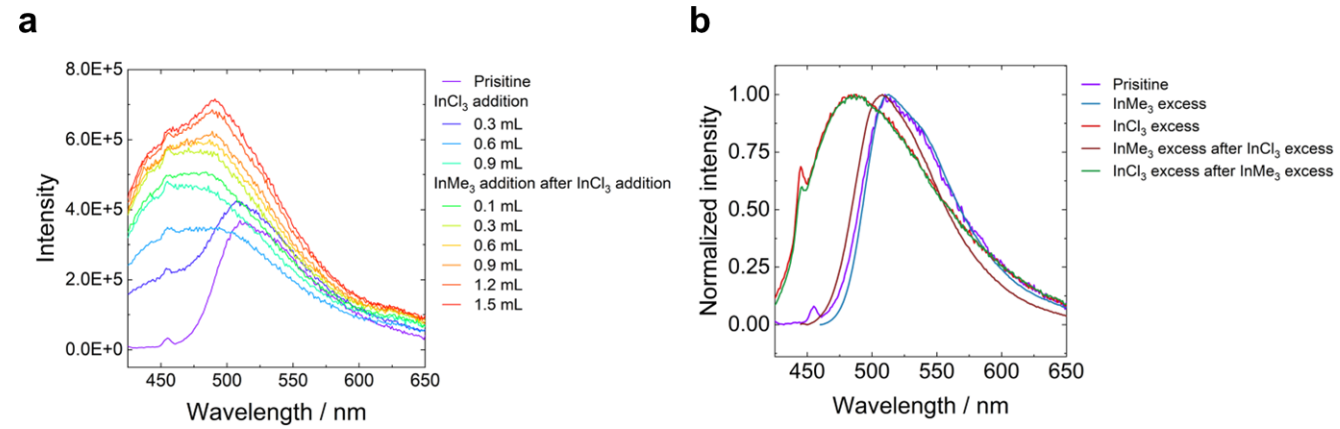

Figure S11. The changes in photoluminescence spectra of a 1.0×10^{-5} M solution of **PhInMe** with (a) stepwise additions and (b) excess additions of $InCl_3$ and/or $InMe_3$.

Table S1. Changes of optical properties of indium complexes in the solution states with the excess addition of $InCl_3$ and/or $InMe_3$

	λ_{abs} / nm	ε / 10^4 M^{-1} cm^{-1} [a]	λ_{ex} / nm [b]	λ_{PL} / nm [c]
Pristine	435	3.9	511	442
Excess $InCl_3$	392	5.0	488	404
Excess $InMe_3$	443	3.9	513	445
Excess $InCl_3$ after excess $InMe_3$	392	7.1	486	402
Excess $InMe_3$ after excess $InCl_3$	432	3.3	508	431

[a] Molar absorption coefficient at the absorption maxima. [b] Detected at λ_{em}. [c] Excited at λ_{abs}.

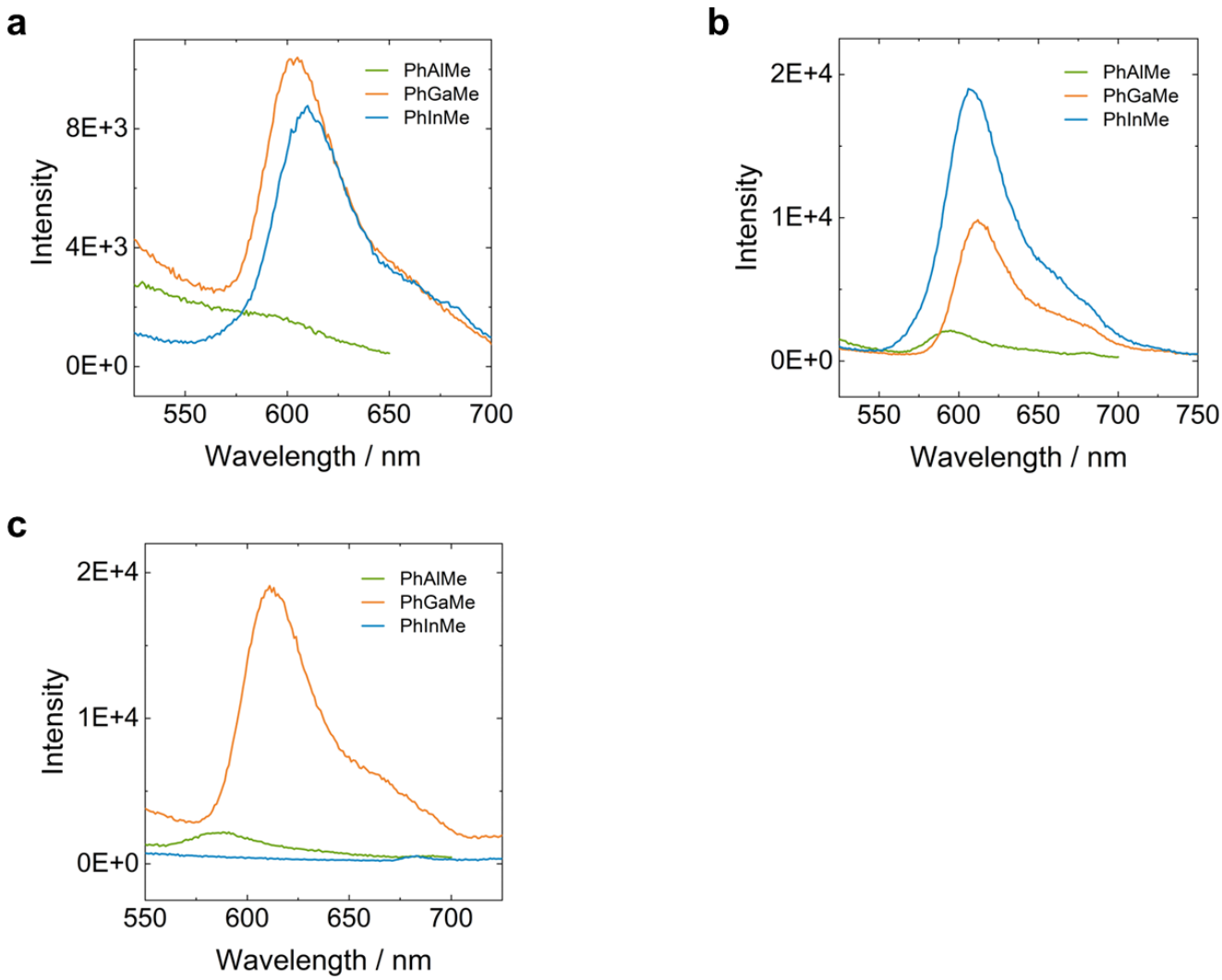

Figure S12. Phosphorescence spectra of the synthesized complexes in (a) 2-MP, (b) MCH, and (c) 2-MTHF solution (1.0×10^{-5} M) at 77 K. These spectra were recorded 1 ms after photoexcitation. Excited at absorption maxima of each solution at room temperature.

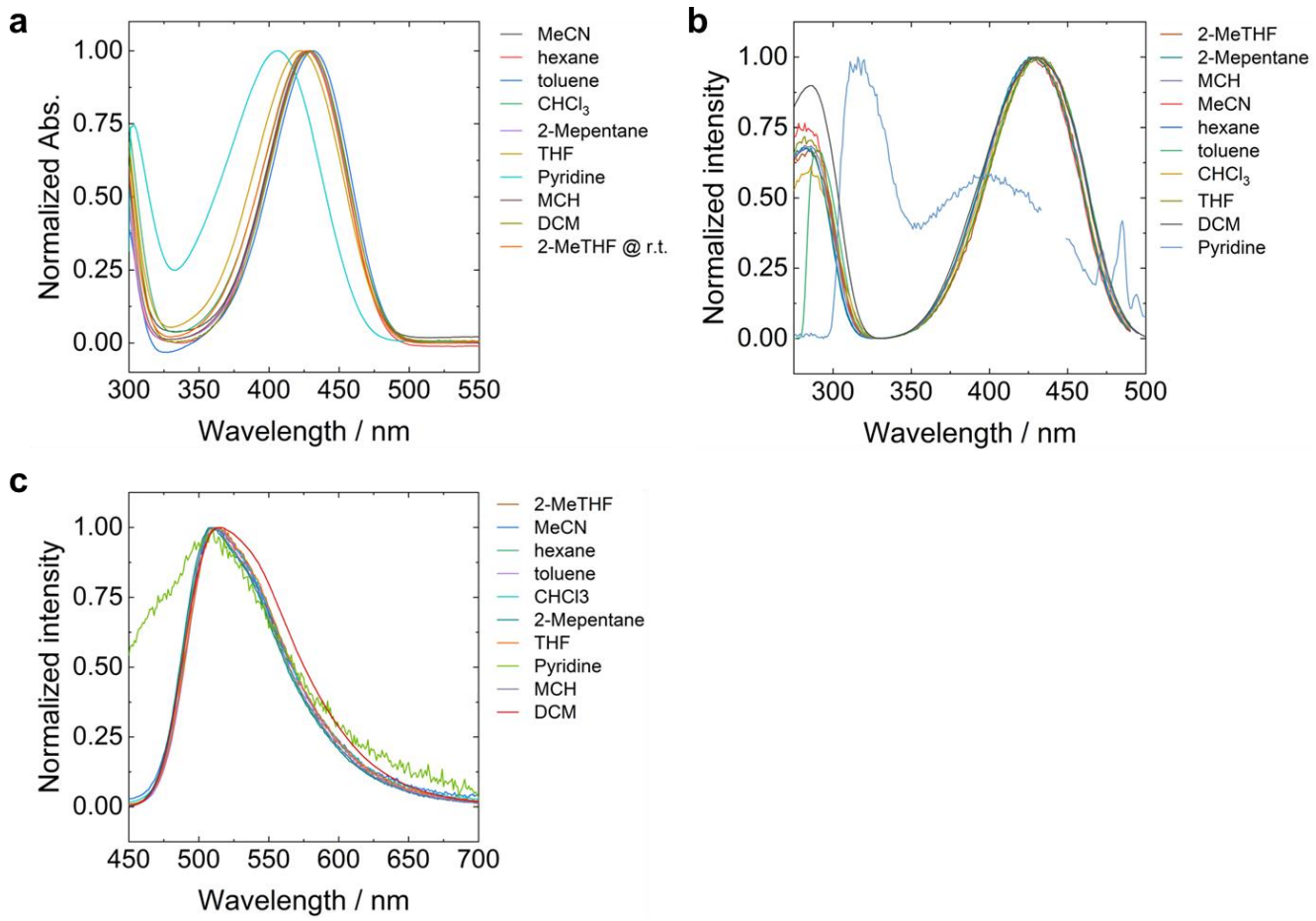

Figure S13. Normalized (a) absorption, (b) excitation, and (c) photoluminescence spectra of **PhAlMe** in various solutions (1.0×10^{-5} M) at room temperature. Excited at each absorption maximum.

Table S2. Optical properties of **PhAlMe** in various solvents

	λ_{abs} / nm	ε / 10^4 M^{-1} cm^{-1} [a]	λ_{ex} / nm [b]	λ_{PL} / nm [c]	Φ_{PL} [d]	τ / ns [b,e]	k_r / 10^8 s^{-1} [f]	k_{nr} / 10^8 s^{-1} [f]
Hexane	428	2.4	425	509	0.13	1.0 (100%)	1.3	8.6
MCH	430	2.8	431	509	0.19	1.3 (100%)	1.5	6.1
2-MP	429	2.3	426	510	0.16	1.2 (96%) 6.1 (4.0%)	1.1	6.1
Toluene	432	2.6	430	511	0.17	1.0 (100%)	1.6	8.1
$CHCl_3$	427	2.2	429	513	0.11	0.34 (47%) 0.96 (52%) 5.2 (1.0%)	1.5	12
2-MTHF	427	1.8	430	512	0.057	0.49 (73%) 0.70 (27%)	1.0	17
THF	423	3.1	431	513	0.056	0.36 (23%) 0.62 (77%)	1.0	17
Pyridine	406	3.1	399	510	< 0.01	1.3 (47%) 7.2 (53%)	< 0.1	> 1.0
DCM	431	1.9	430	515	0.087	0.095 (14%) 0.61 (86%)	1.6	17
MeCN	428	2.3	428	512	0.030	0.24 (100%)	1.3	41

[a] Molar absorption coefficient at the absorption maxima. [b] Detected at λ_{em}. [c] Excited at λ_{abs}. [d] Determined with the integrated sphere method. [e] Excited at 369 nm. [f] k_r and k_{nr} were determined from the following formula: $k_r = \Phi_{PL} / \langle\tau\rangle$ and $k_{nr} = (1 - \Phi_{PL}) / \langle\tau\rangle$, where $\langle\tau\rangle = \Sigma\alpha_i\tau_i^2 / \Sigma\alpha_i\tau_i = \Sigma f_i\tau_i$.

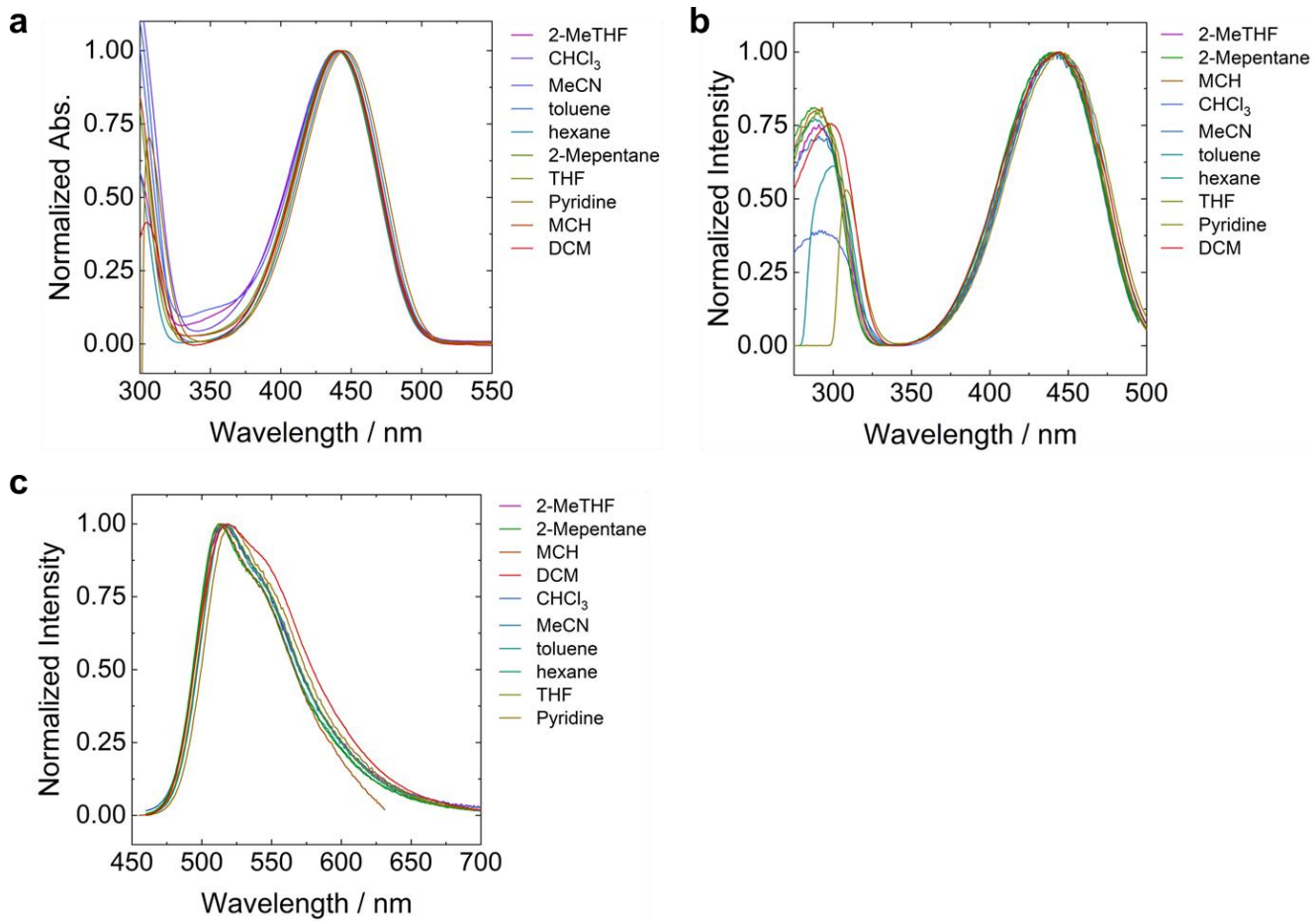

Figure S14. Normalized (a) absorption, (b) excitation, and (c) photoluminescence spectra of **PhGaMe** in various solutions (1.0×10^{-5} M) at room temperature. Excited at each absorption maximum.

Table S3. Optical properties of **PhGaMe** in various solvents

	λ_{abs} / nm	ε / 10^4 M^{-1} cm^{-1} [a]	λ_{ex} / nm [b]	λ_{PL} / nm [c]	Φ_{PL} [d]	τ / ns [b,e]	k_r / 10^8 s^{-1} [f]	k_{nr} / 10^8 s^{-1} [f]
Hexane	441	2.3	442	512	0.18	1.3 (98%) 7.2 (2.0%)	1.2	5.8
MCH	442	1.9	445	513	0.22	0.15 (15%) 4.7 (86%)	1.5	5.5
2-MP	441	2.5	443	512	0.17	1.3 (96%) 6.6 (4.1%)	1.2	5.6
Toluene	444	2.4	444	516	0.19	1.4 (98.2%) 7.6 (1.8%)	1.2	5.2
$CHCl_3$	440	2.3	445	518	0.15	1.1 (99%) 6.8 (1.0%)	1.3	7.6
2-MTHF	440	1.9	443	515	0.10	0.67 (100%)	1.5	13
THF	442	2.2	444	516	0.11	0.63 (57%) 0.83 (43%)	1.5	13
Pyridine	445	2.0	445	519	0.13	0.80 (100%)	1.6	11
DCM	441	1.7	445	518	0.10	0.41 (1.0%) 0.73 (99%)	1.4	12
MeCN	440	2.1	442	514	0.04	0.36 (99%) 6.5 (1%)	1.1	25

[a] Molar absorption coefficient at the absorption maxima. [b] Detected at λ_{em}. [c] Excited at λ_{abs}. [d] Determined with the integrated sphere method. [e] Excited at 369 nm. [f] k_r and k_{nr} were determined from the following formula: $k_r = \Phi_{PL} / \langle\tau\rangle$ and $k_{nr} = (1 - \Phi_{PL}) / \langle\tau\rangle$, where $\langle\tau\rangle = \Sigma\alpha_i\tau_i^2 / \Sigma\alpha_i\tau_i = \Sigma f_i\tau_i$.

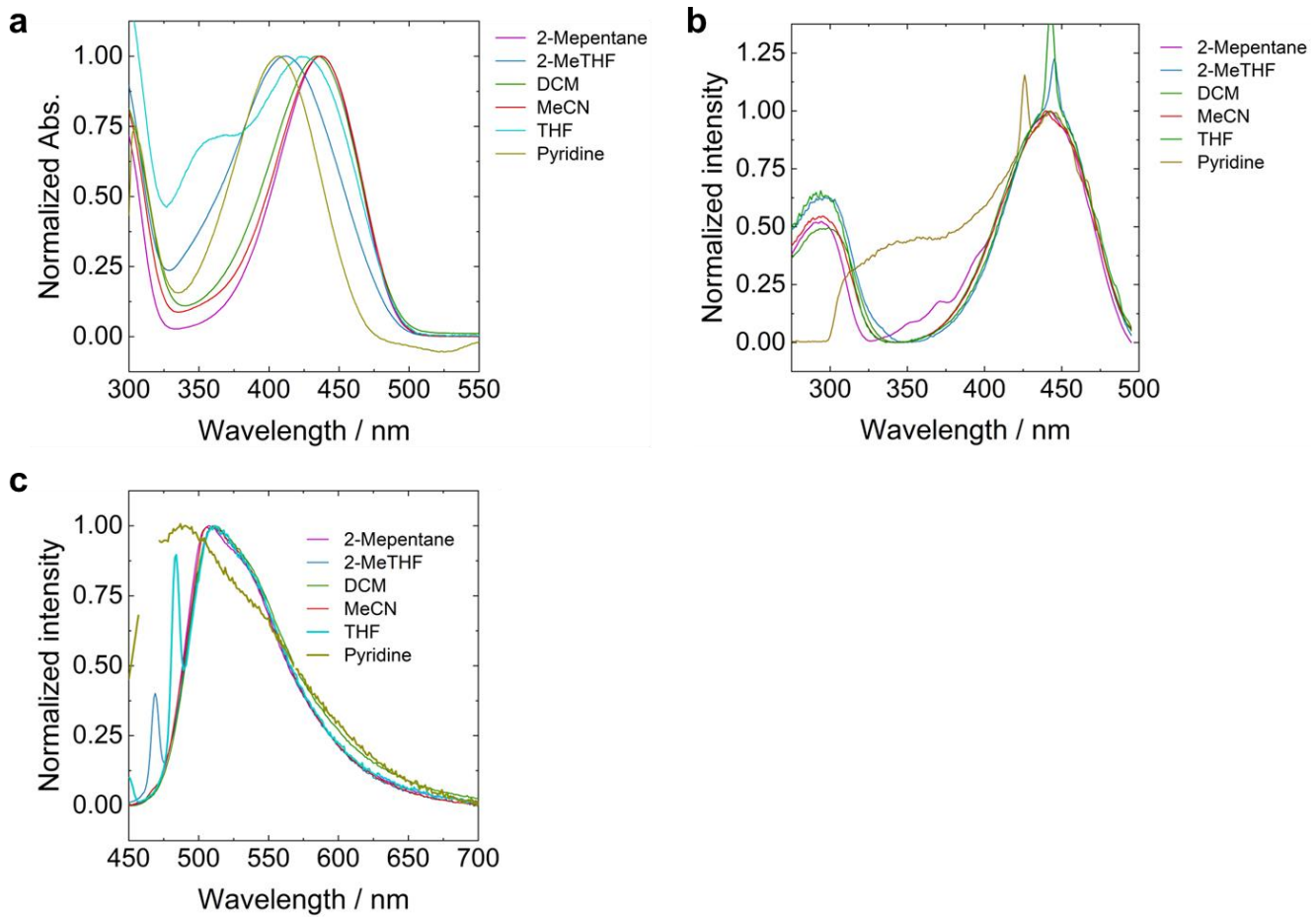

Figure S15. Normalized (a) absorption, (b) excitation, and (c) photoluminescence spectra of **PhInMe** in various solutions (1.0×10^{-5} M) at room temperature. Excited at each absorption maximum.

Table S4. Optical properties of **PhInMe** in various solvents

	λ_{abs} / nm	ε / 10^4 M^{-1} cm^{-1} [a]	λ_{ex} / nm [b]	λ_{PL} / nm [c]	Φ_{PL} [d]	τ / ns [b,e]	k_r / 10^8 s^{-1} [f]	k_{nr} / 10^8 s^{-1} [f]
2-MP	437	2.11	442	508	< 0.01	0.059 (42%) 1.0 (58%)	< 1.0	> 100
2-MTHF	412	1.51	441	512	< 0.01	0.042 (76%) 1.5 (14%) 8.7 (10%)	< 1.0	> 100
THF	410	1.2	437	494	< 0.01	1.3 (62%) 8.8 (38%)	< 1.0	> 100
Pyridine	406	1.1	443	473	< 0.01	1.6 (56%) 8.7 (44%)	< 1.0	> 100
DCM	443	1.60	442	513	< 0.01	0.052 (99%) 0.28 (1.0%)	< 1.0	> 100
MeCN	437	1.86	440	506	< 0.01	0.021 (99%) 0.24 (1.0%)	< 1.0	> 100

[a] Molar absorption coefficient at the absorption maxima. [b] Detected at λ_{em}. [c] Excited at λ_{abs}. [d] Determined with the integrated sphere method. [e] Excited at 369 nm. [f] k_r and k_{nr} were determined from the following formula: $k_r = \Phi_{PL} / \langle\tau\rangle$ and $k_{nr} = (1 - \Phi_{PL}) / \langle\tau\rangle$, where $\langle\tau\rangle = \Sigma\alpha_i\tau_i^2 / \Sigma\alpha_i\tau_i = \Sigma f_i\tau_i$.

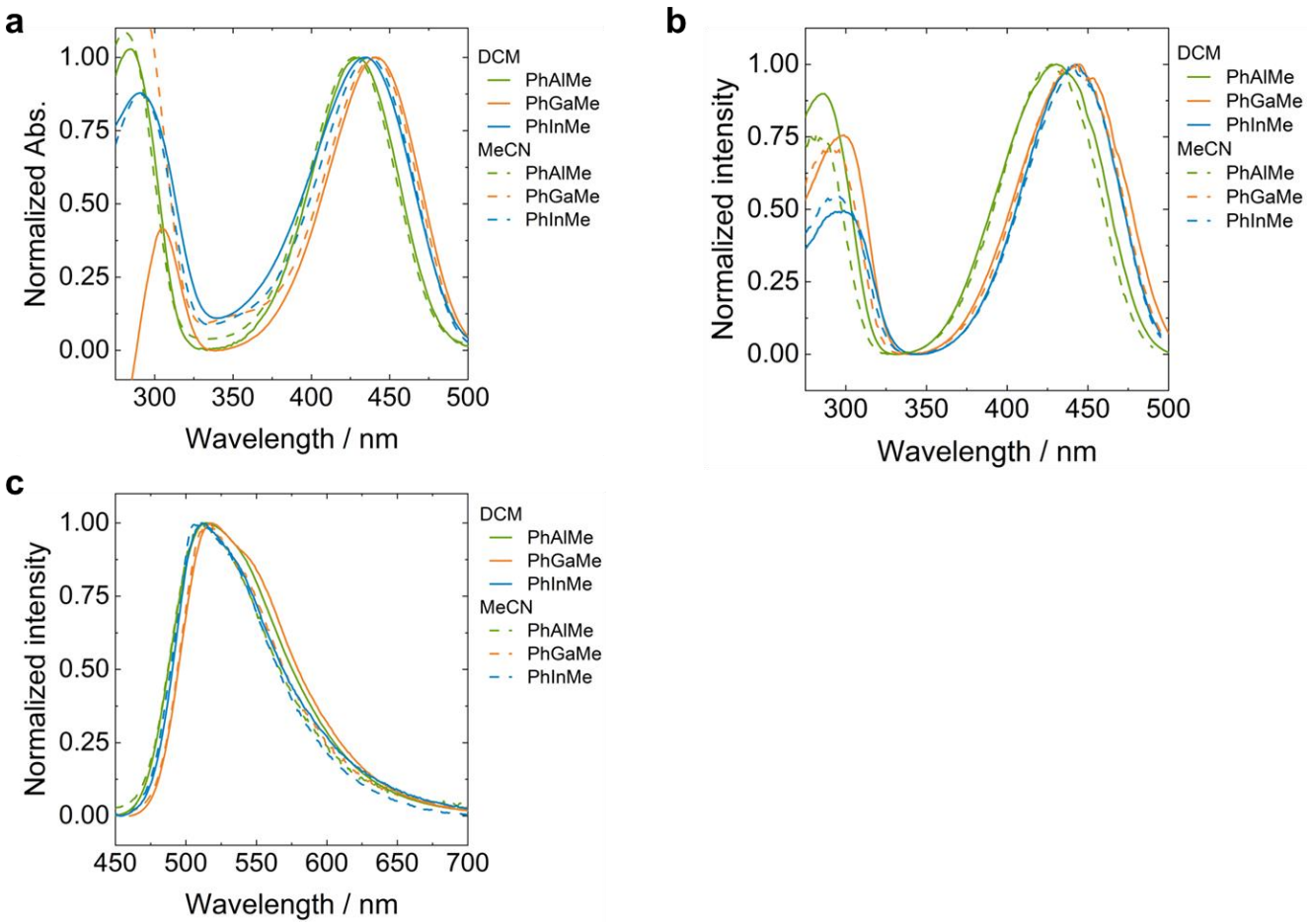

Figure S16. Normalized (a) absorption, (b) excitation, and (c) photoluminescence spectra (excited at each absorption spectra) of the synthesized complexes in 1.0×10^{-5} M CH_2Cl_2 (solid lines) and MeCN (dashed lines) solutions at room temperature.

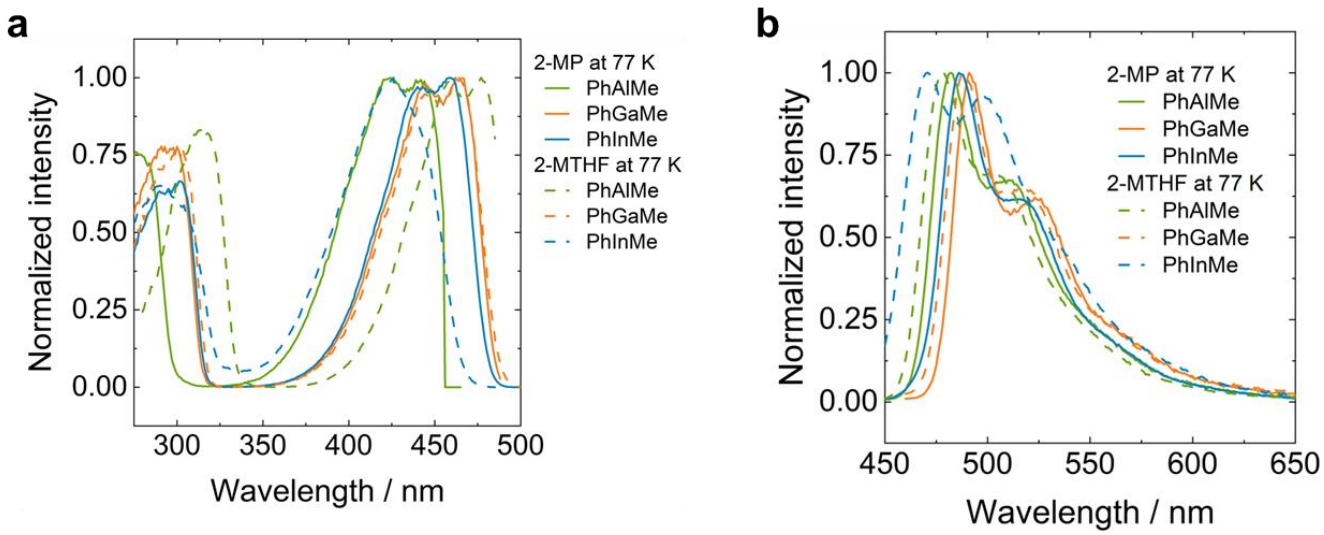

Figure S17. Normalized (a) excitation and (b) photoluminescence spectra (excited at each absorption spectra at room temperature) of the synthesized complexes in 1.0×10^{-5} M 2-MP (solid lines) and 2-MTHF (dashed lines) solutions at 77 K.

Table S5. Optical properties of dialdiminate complexes in 2-MP or 2-MTHF (1.0×10^{-5} M) at 77 K

		λ_{ex} / nm [a]	λ_{PL} / nm [b]	Φ_{PL} [c]	τ / ns [a,d]	k_r / 10^8 s^{-1} [e]	k_{nr} / 10^8 s^{-1} [e]
PhAlMe	2-MP	449	482	0.98	4.4 (51%) 6.4 (49%)	1.8	0.046
	2-MTHF	442	477	0.55	2.8 (6.0%) 4.8 (94%)	1.2	0.97
PhGaMe	2-MP	467	491	0.90	5.1 (81%) 9.1 (19%)	1.5	0.18
	2-MTHF	464	489	0.87	0.71 (2.0%) 4.7 (98%)	2.1	0.31
PhInMe	2-MP	460	486	0.55	2.0 (5.0%) 4.2 (95%)	1.4	1.1
	2-MTHF	426	471	0.076	1.2 (19%) 3.8 (81%)	0.23	2.8

[a] Detected at λ_{em}. [b] Excited at λ_{abs}. [c] Determined with the integrated sphere method. [d] Excited at 369 nm. [e] k_r and k_{nr} were determined from the following formula: $k_r = \Phi_{PL} / \langle\tau\rangle$ and $k_{nr} = (1 - \Phi_{PL}) / \langle\tau\rangle$, where $\langle\tau\rangle = \Sigma\alpha_i\tau_i^2 / \Sigma\alpha_i\tau_i = \Sigma f_i\tau_i$.

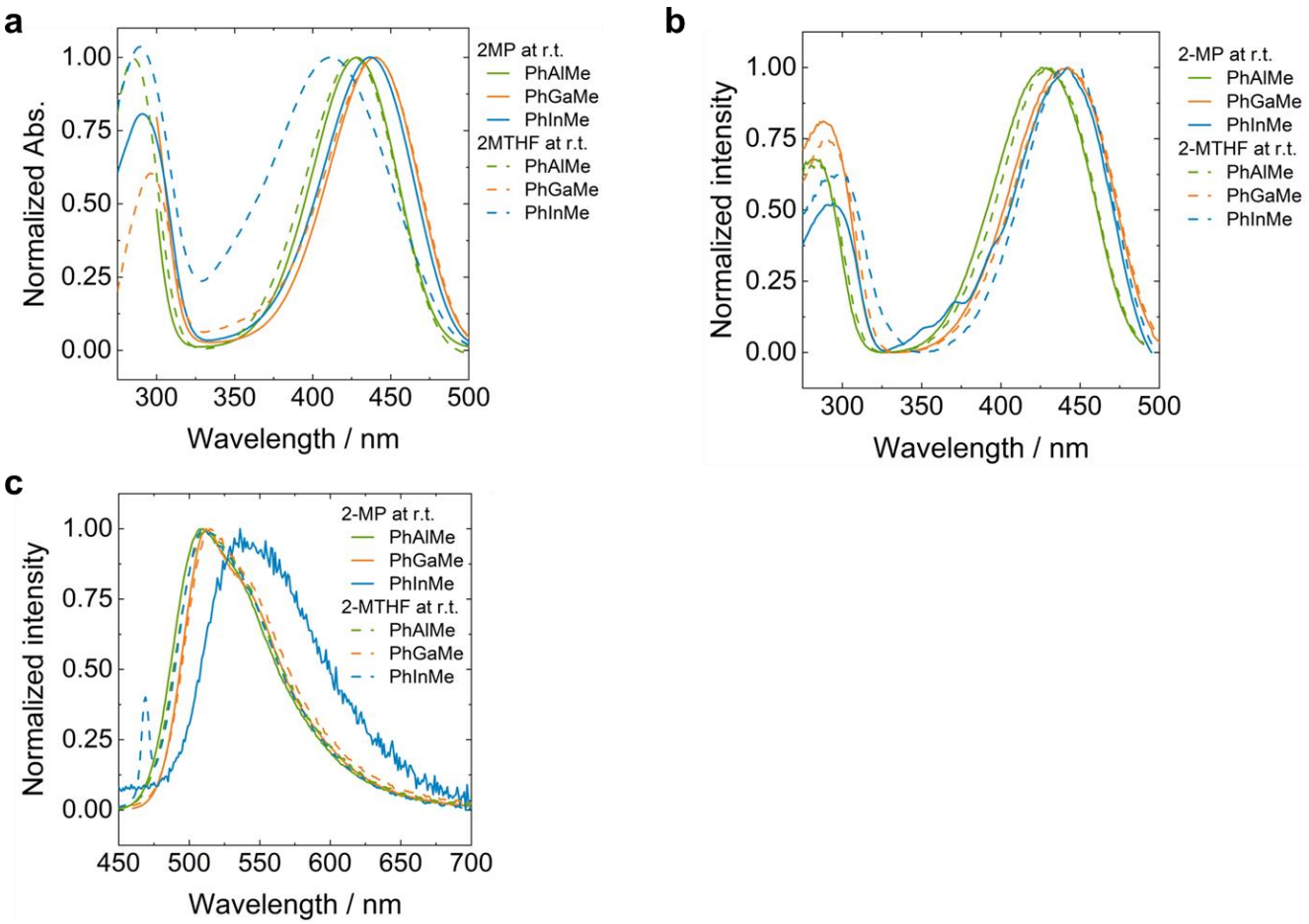

Figure S18. Normalized (a) absorption, (b) excitation, and (c) photoluminescence spectra (excited at each absorption spectra) of the synthesized complexes in 1.0×10^{-5} M 2-MP (solid lines) and 2-MTHF (dashed lines) solutions at room temperature.

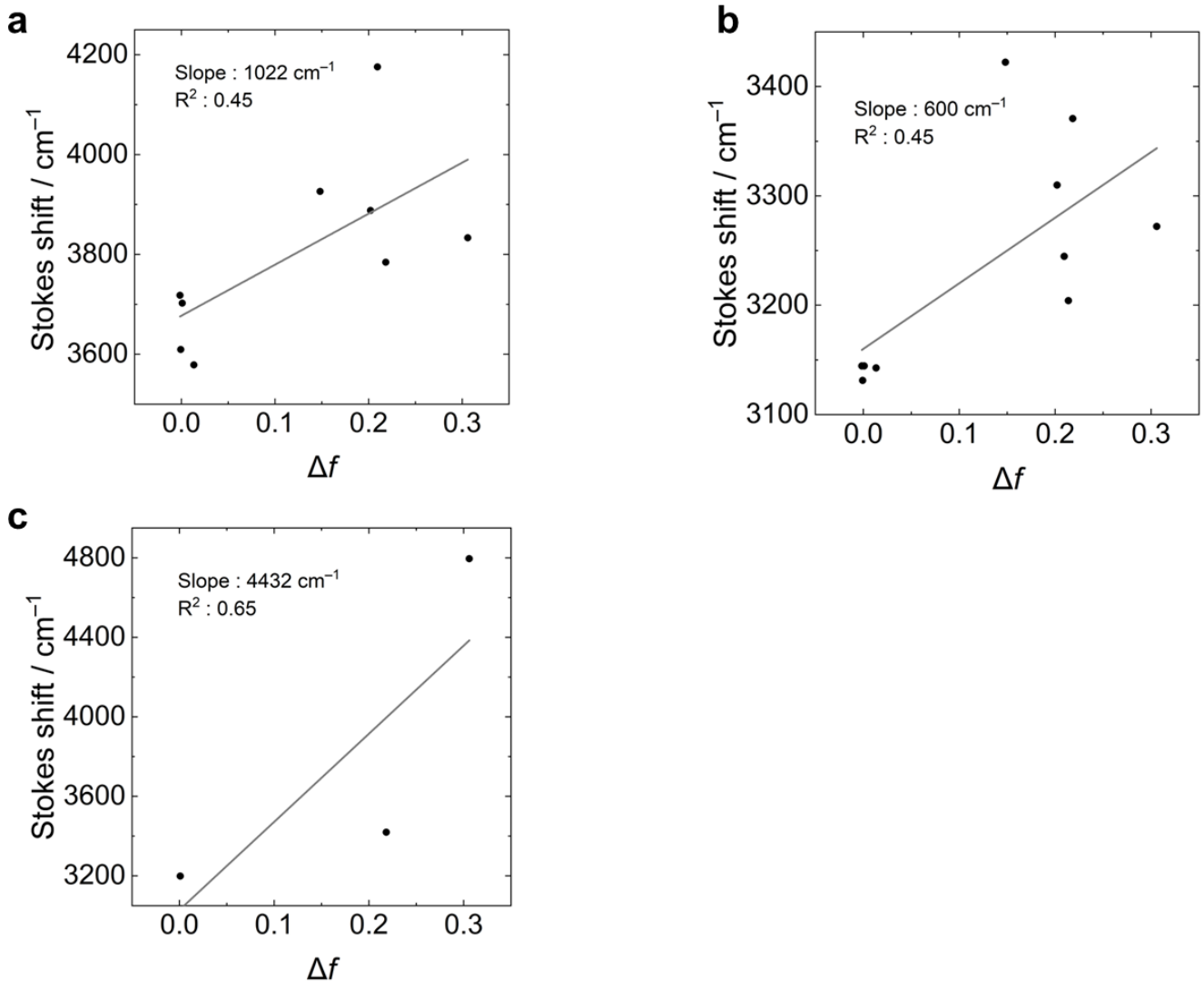

Figure S19. Lippert–Mataga plots[19] for (a) **PhAlMe**, (b) **PhGaMe** and (c) **PhInMe**. Filled circles and solid lines represent measured data and fitted lines, respectively.

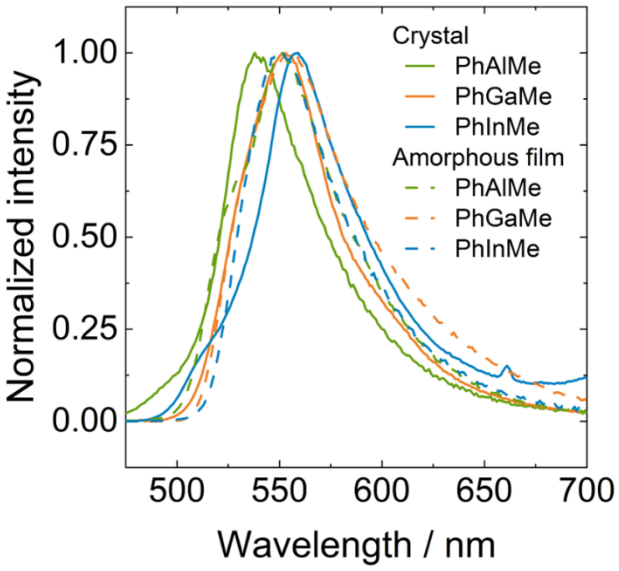

Figure S20. Normalized photoluminescence spectra of the synthesized complexes in their solid states (excited at each absorption maximum of CH_2Cl_2 solution at room temperature).

Table S6. The optical properties of dialdiminate complexes in the solid states [a]

		λ_{PL} / nm [b]	Φ_{PL} [c]	τ / ns [d,e]	k_r / 10^8 s^{-1} [f]	k_{nr} / 10^8 s^{-1} [f]
PhAlMe	Amorphous film	551	0.15	0.58 (18%) 1.5 (82%)	1.1	6.5
	Crystal	538	0.32	1.0 (7.0%) 3.7 (93%)	1.0	2.2
PhGaMe	Amorphous film	556	0.14	0.28 (40%) 1.5 (60%)	1.4	8.7
	Crystal	552	0.49	1.8 (23%) 4.5 (77%)	2.2	2.3
PhInMe	Amorphous film	550	0.016	0.14 (77%) 0.99 (23%)	0.38	23
	Crystal	560	0.30	1.5 (9.0%) 3.8 (91%)	0.83	1.9

[a] Amorphous samples were prepared on quartz substrates by the drop-casting method with the DCM solutions. [b] Excited at λ_{abs}. [c] Determined with the integrated sphere method. [d] Excited at 369 nm. [e] Detected at λ_{em}. [f] k_r and k_{nr} were determined from the following formula: $k_r = \Phi_{PL} / \langle\tau\rangle$ and $k_{nr} = (1 - \Phi_{PL}) / \langle\tau\rangle$, where $\langle\tau\rangle = \Sigma\alpha_i\tau_i^2 / \Sigma\alpha_i\tau_i = \Sigma f_i\tau_i$.

DFT calculations

Table S7. Calculated parameters of the electronic transitions at the S_1 state for single molecules of the indium dialdiminates [a]

	Composition [b]	Coefficient [c]	E / eV	λ / nm	f [d]
PhInCl	HOMO→LUMO	0.690	2.99	415	0.740
PhInMeCl	HOMO→LUMO	0.691	2.99	415	0.729
PhInMe	HOMO→LUMO	0.687	2.97	417	0.707

[a] Calculated at the level with PBE1PBE/6-31+G(d,p) (for C, H, N, and Cl) and LanL2DZ (for In). [b] Composition of the electronic states. [c] Coefficient for the electronic transition. [d] Oscillator strength.

Table S8. Calculated parameters of the electronic transitions at the S_1 state for single molecules of **PhAlMe** and **PhGaMe** [a]

	Composition [b]	Coefficient [c]	E / eV	λ / nm	f [d]
PhAlMe	HOMO→LUMO	0.679	2.85	434	0.494
PhGaMe	HOMO→LUMO	0.687	3.38	367	0.513

[a] Calculated at the level with PBE1PBE/6-31+G(d,p). [b] Composition of the electronic states. [c] Coefficient for the electronic transition. [d] Oscillator strength.

Table S9. Calculated parameters of the electronic transitions at the S_1 state for single molecules of **PhGaMe** and **PhInMe** [a]

	Composition [b]	Coefficient [c]	E / eV	λ / nm	f [d]
PhGaMe	HOMO→LUMO	0.686	3.42	363	0.536
PhInMe	HOMO→LUMO	0.687	2.97	417	0.707

[a] Calculated at the level with PBE1PBE/6-31+G(d,p) (for C, H, N) and LanL2DZ (for Ga and In). [b] Composition of the electronic states. [c] Coefficient for the electronic transition. [d] Oscillator strength.

Table S10. Calculated parameters of the electronic transitions at the S_0 state for the DFT-optimized and single-crystal structures of **PhAlMe** and **PhGaMe** [a]

		Composition [b]	Coefficient [c]	E / eV	λ / nm	f [d]
PhAlMe	Optimized	HOMO→LUMO	0.680	3.41	364	0.471
	SC monomer	HOMO–1→LUMO HOMO→LUMO	–0.211 0.664	3.21	387	0.316
	SC dimer	$HOMO_1$→$LUMO_1$ $HOMO_2$→$LUMO_1$ $HOMO_2$→$LUMO_2$	–0.170 0.671 0.117	3.06	405	0.016
PhGaMe	Optimized	HOMO→LUMO	0.687	3.37	368	0.528
	SC monomer	HOMO–1→LUMO HOMO→LUMO	–0.121 0.682	3.27	379	0.426
	SC dimer	$HOMO_1$→$LUMO_1$ $HOMO_2$→$LUMO_1$ $HOMO_2$→$LUMO_2$	–0.208 0.649 0.155	2.85	435	0.034

[a] Calculated at the level with PBE1PBE/6-31G(d,p). [b] Composition of the electronic states. [c] Coefficient for the electronic transition. [d] Oscillator strength.

Table S11. Calculated parameters of the electronic transitions at the S_0 state for the DFT-optimized and single-crystal structures of **PhGaMe** and **PhInMe** [a]

		Composition [b]	Coefficient [c]	E / eV	λ / nm	f [d]
PhGaMe	Optimized	HOMO→LUMO	0.687	3.42	362	0.564
	SC monomer	HOMO–1→LUMO HOMO→LUMO	–0.121 0.681	3.32	373	0.457
	SC dimer	$HOMO_1$→$LUMO_1$ $HOMO_2$→$LUMO_1$ $HOMO_2$→$LUMO_2$	–0.224 0.638 0.172	2.88	431	0.031
PhInMe	Optimized	HOMO→LUMO	0.683	3.46	358	0.647
	SC monomer	HOMO–1→LUMO HOMO→LUMO	–0.102 0.684	3.35	370	0.660
	SC dimer	$HOMO_1$→$LUMO_1$ $HOMO_2$→$LUMO_1$ $HOMO_2$→$LUMO_2$	–0.187 0.667 –0.126	3.03	409	0.010

[a] Calculated at the level with PBE1PBE/6-31G(d,p) (for C, H, N) and LanL2DZ (for Ga and In). [b] Composition of the electronic states. [c] Coefficient for the electronic transition. [d] Oscillator strength.

Table S12. Atomic coordinates of the optimized structure for **PhAlMe** in the gas phase

Center Number	Atomic Number	Atomic Type	Coordinates (Å)		
			x	y	z
1	6	0	0.017497	-1.75412	0.837213
2	6	0	1.129652	-1.92872	0.012359
3	6	0	1.53578	-0.88218	-0.81683
4	6	0	0.832195	0.321308	-0.828
5	6	0	-0.28492	0.518036	0.003701
6	6	0	-0.67441	-0.54384	0.839828
7	1	0	-0.30394	-2.55657	1.495216
8	1	0	1.673138	-2.86875	0.0157
9	1	0	2.393584	-1.00748	-1.47157
10	1	0	1.136017	1.110706	-1.50986
11	1	0	-1.51223	-0.40958	1.518373
12	6	0	-1.02972	1.805916	-0.00073
13	6	0	-2.43476	1.768798	0.030063
14	6	0	-0.29686	3.005142	-0.03649
15	1	0	-2.89082	0.778134	0.023346
16	1	0	0.78927	2.906524	-0.02854
17	6	0	0.166017	5.314001	-0.00098
18	6	0	1.205901	5.305366	0.941553
19	6	0	0.035351	6.409958	-0.86632
20	6	0	2.110968	6.364242	0.998091
21	1	0	1.283735	4.483211	1.646161
22	6	0	0.940476	7.467859	-0.79758
23	1	0	-0.76052	6.415065	-1.60313
24	6	0	1.983689	7.449337	0.129872
25	1	0	2.908349	6.346073	1.735285
26	1	0	0.832334	8.306399	-1.47916
27	1	0	2.685795	8.275783	0.180578
28	6	0	-4.66657	2.519758	-0.01841
29	6	0	-5.55557	3.185266	0.838244
30	6	0	-5.1734	1.609278	-0.95863
31	6	0	-6.92375	2.929174	0.76344
32	1	0	-5.16668	3.881429	1.57346
33	6	0	-6.54244	1.353727	-1.02118
34	1	0	-4.49634	1.127383	-1.65708

35	6	0	-7.4237	2.010858	-0.16151
36	1	0	-7.59989	3.445625	1.438362
37	1	0	-6.92095	0.649733	-1.75652
38	1	0	-8.49006	1.815083	-0.21698
39	7	0	-0.77679	4.243274	-0.07625
40	7	0	-3.26867	2.802428	0.063175
41	13	0	-2.70023	4.694784	-0.00346
42	6	0	-3.37245	5.472519	-1.69635
43	1	0	-4.45441	5.314933	-1.79557
44	1	0	-3.2163	6.557366	-1.75488
45	1	0	-2.91037	5.030212	-2.58832
46	6	0	-3.03428	5.656479	1.69545
47	1	0	-4.04484	6.081444	1.74939
48	1	0	-2.90116	5.024165	2.582729
49	1	0	-2.34217	6.501176	1.80865

Table S13. Atomic coordinates of the optimized structure for **PhGaMe** in the gas phase

Center Number	Atomic Number	Atomic Type	Coordinates (Å)		
			x	y	z
1	6	0	1.298706	-0.927751	0.835768
2	6	0	2.411054	-1.102336	0.011191
3	6	0	2.81659	-0.054884	-0.817132
4	6	0	2.11269	1.148341	-0.827697
5	6	0	0.995018	1.345959	0.003692
6	6	0	0.606744	0.282426	0.838936
7	1	0	0.977131	-1.730287	1.493686
8	1	0	2.9547	-2.042287	0.014054
9	1	0	3.674324	-0.179349	-1.472213
10	1	0	2.416456	1.937091	-1.510298
11	1	0	-0.230219	0.415567	1.518713
12	6	0	0.250395	2.633223	-0.000293
13	6	0	-1.155417	2.591251	0.046382
14	6	0	0.987815	3.830692	-0.050615
15	1	0	-1.606501	1.597661	0.0487
16	1	0	2.07401	3.726233	-0.049745
17	6	0	-3.389303	3.348945	-0.006508
18	6	0	-4.277783	4.060274	0.814406
19	6	0	-3.903941	2.435023	-0.939378
20	6	0	-5.648217	3.822167	0.734022
21	1	0	-3.885257	4.757937	1.546264
22	6	0	-5.276396	2.201596	-1.011289
23	1	0	-3.227528	1.925513	-1.618562
24	6	0	-6.155411	2.893179	-0.176677
25	1	0	-6.32301	4.36626	1.3884
26	1	0	-5.659454	1.490222	-1.737201
27	1	0	-7.22437	2.714353	-0.238645
28	6	0	1.444919	6.144981	-0.007553
29	6	0	2.491534	6.139566	0.927841
30	6	0	1.273364	7.265988	-0.834085
31	6	0	3.378193	7.21304	0.996828
32	1	0	2.594105	5.302279	1.611107
33	6	0	2.163078	8.335406	-0.756614
34	1	0	0.474556	7.270281	-1.567783

35	6	0	3.219104	8.315917	0.156658
36	1	0	4.184124	7.193702	1.724724
37	1	0	2.029625	9.188625	-1.41525
38	1	0	3.907085	9.153545	0.216293
39	7	0	-1.996175	3.613042	0.081842
40	7	0	0.521451	5.068778	-0.09299
41	31	0	-1.437193	5.550074	-0.009295
42	6	0	-1.696615	6.485963	1.72597
43	1	0	-0.972639	7.302418	1.825632
44	1	0	-2.693337	6.932879	1.81046
45	1	0	-1.55277	5.817332	2.581676
46	6	0	-2.114171	6.234115	-1.749412
47	1	0	-2.002987	7.32039	-1.838702
48	1	0	-1.604776	5.771465	-2.601743
49	1	0	-3.182901	6.014524	-1.850652

Table S14. Atomic coordinates of the optimized structure for **PhInMe** in the gas phase

Center Number	Atomic Number	Atomic Type	Coordinates (Å)		
			x	y	z
1	6	0	0.058	-1.6945	0.900714
2	6	0	1.112753	-1.90013	0.008193
3	6	0	1.462831	-0.88685	-0.88741
4	6	0	0.759236	0.317892	-0.89691
5	6	0	-0.29903	0.541892	0.002021
6	6	0	-0.63496	-0.48357	0.90411
7	1	0	-0.21428	-2.47108	1.60662
8	1	0	1.655139	-2.83832	0.010564
9	1	0	2.273229	-1.04108	-1.59096
10	1	0	1.010095	1.083773	-1.62249
11	1	0	-1.42543	-0.31604	1.627334
12	6	0	-1.04677	1.835295	-0.00125
13	6	0	-2.45081	1.761858	0.02194
14	6	0	-0.28246	3.0153	-0.02723
15	1	0	-2.85722	0.748863	0.014321
16	1	0	0.798184	2.862044	-0.01666
17	6	0	0.27935	5.322676	0.024586
18	6	0	1.367969	5.243832	0.908631
19	6	0	0.134612	6.467205	-0.77665
20	6	0	2.296872	6.281755	0.976984
21	1	0	1.46164	4.387969	1.566051
22	6	0	1.063505	7.503302	-0.69901
23	1	0	-0.68923	6.524971	-1.47891
24	6	0	2.150454	7.415409	0.17476
25	1	0	3.126963	6.210467	1.670376
26	1	0	0.942781	8.3768	-1.32918
27	1	0	2.869766	8.22322	0.234423
28	6	0	-4.73061	2.426166	-0.03739
29	6	0	-5.65198	3.125749	0.759185
30	6	0	-5.20357	1.440074	-0.91873
31	6	0	-7.01321	2.837484	0.679667
32	1	0	-5.29247	3.871179	1.459409
33	6	0	-6.56641	1.152748	-0.98897
34	1	0	-4.50719	0.929334	-1.5727

35	6	0	-7.47752	1.848363	-0.19137
36	1	0	-7.71131	3.380364	1.306253
37	1	0	-6.91733	0.395189	-1.68026
38	1	0	-8.53638	1.627876	-0.25251
39	7	0	-0.7037	4.280199	-0.06149
40	7	0	-3.33684	2.758211	0.050479
41	49	0	-2.81918	4.901118	-0.00902
42	6	0	-3.43736	5.664114	-1.97179
43	1	0	-4.48688	5.409356	-2.15969
44	1	0	-3.33816	6.754209	-2.02678
45	1	0	-2.83202	5.215785	-2.76845
46	6	0	-3.17624	5.825048	1.949457
47	1	0	-4.17055	6.283213	2.000527
48	1	0	-3.09151	5.079793	2.749163
49	1	0	-2.4322	6.608169	2.136

Table S15. Summary of natural population analysis for **PhAlMe** in the gas phase[a]

Center Number	Atomic Number	Natural charge	Natural Population			
			Core	Valence	Rydberg	Total
1	6	-0.23978	1.99911	4.22695	0.01372	6.23978
2	6	-0.25671	1.99911	4.2442	0.0134	6.25671
3	6	-0.23979	1.99911	4.22695	0.01372	6.23979
4	6	-0.24919	1.99906	4.23751	0.01263	6.24919
5	6	-0.04263	1.99903	4.02848	0.01512	6.04263
6	6	-0.2492	1.99906	4.23751	0.01263	6.2492
7	1	0.25134	0	0.7473	0.00135	0.74866
8	1	0.25066	0	0.74803	0.00131	0.74934
9	1	0.25134	0	0.74731	0.00135	0.74866
10	1	0.2492	0	0.74928	0.00152	0.7508
11	1	0.24923	0	0.74925	0.00152	0.75077
12	6	-0.23906	1.99899	4.22388	0.01619	6.23906
13	6	0.12621	1.99915	3.85527	0.01936	5.87379
14	6	0.12632	1.99915	3.85517	0.01936	5.87368
15	1	0.238	0	0.75998	0.00202	0.762
16	1	0.238	0	0.75998	0.00201	0.762
17	6	0.14476	1.99896	3.8376	0.01868	5.85524
18	6	-0.27209	1.99903	4.26069	0.01238	6.27209
19	6	-0.25894	1.99904	4.24691	0.01299	6.25894
20	6	-0.23607	1.99912	4.22315	0.01381	6.23607
21	1	0.25732	0	0.74125	0.00143	0.74268
22	6	-0.23466	1.99912	4.22178	0.01376	6.23466
23	1	0.26596	0	0.73245	0.00159	0.73404
24	6	-0.25561	1.99911	4.24316	0.01334	6.25561
25	1	0.25409	0	0.74457	0.00135	0.74591
26	1	0.25475	0	0.74393	0.00132	0.74525
27	1	0.25284	0	0.74588	0.00129	0.74716
28	6	0.14502	1.99896	3.83736	0.01867	5.85498
29	6	-0.25908	1.99904	4.24705	0.013	6.25908
30	6	-0.27215	1.99903	4.26075	0.01238	6.27215
31	6	-0.23462	1.99912	4.22173	0.01377	6.23462
32	1	0.26591	0	0.7325	0.00159	0.73409
33	6	-0.23602	1.99912	4.2231	0.01381	6.23602
34	1	0.25726	0	0.74131	0.00143	0.74274

35	6	-0.25565	1.99911	4.2432	0.01334	6.25565
36	1	0.25475	0	0.74393	0.00132	0.74525
37	1	0.25407	0	0.74458	0.00135	0.74593
38	1	0.25283	0	0.74588	0.00129	0.74717
39	7	-0.70393	1.99938	5.68607	0.01847	7.70393
40	7	-0.70388	1.99938	5.68602	0.01848	7.70388
41	13	1.83566	9.9978	1.14711	0.01943	11.16434
42	6	-1.38418	1.99954	5.37238	0.01226	7.38418
43	1	0.26208	0	0.73682	0.00111	0.73792
44	1	0.25198	0	0.74695	0.00107	0.74802
45	1	0.25197	0	0.74665	0.00138	0.74803
46	6	-1.38443	1.99954	5.37263	0.01226	7.38443
47	1	0.25211	0	0.74682	0.00108	0.74789
48	1	0.25194	0	0.74668	0.00138	0.74806
49	1	0.2621	0	0.7368	0.0011	0.7379

[a] Calculated at the level with PBE1PBE/6-31G(d,p)

Table S16. Summary of natural population analysis for **PhGaMe** in the gas phase[a]

Center Number	Atomic Number	Natural charge	Natural Population			
			Core	Valence	Rydberg	Total
1	6	-0.24002	1.99911	4.22719	0.01372	6.24002
2	6	-0.25827	1.99911	4.24575	0.01341	6.25827
3	6	-0.24002	1.99911	4.22719	0.01372	6.24002
4	6	-0.25044	1.99906	4.23875	0.01264	6.25044
5	6	-0.04118	1.99903	4.02701	0.01514	6.04118
6	6	-0.25044	1.99906	4.23875	0.01264	6.25044
7	1	0.25075	0	0.74789	0.00136	0.74925
8	1	0.25009	0	0.74859	0.00132	0.74991
9	1	0.25075	0	0.74789	0.00136	0.74925
10	1	0.24864	0	0.74983	0.00153	0.75136
11	1	0.24864	0	0.74983	0.00153	0.75136
12	6	-0.24178	1.999	4.22639	0.01638	6.24178
13	6	0.12529	1.99915	3.85593	0.01963	5.87471
14	6	0.12528	1.99915	3.85594	0.01963	5.87472
15	1	0.23538	0	0.76252	0.0021	0.76462
16	1	0.23536	0	0.76254	0.0021	0.76464
17	6	0.14796	1.99896	3.83417	0.01891	5.85204
18	6	-0.26141	1.99904	4.24924	0.01313	6.26141
19	6	-0.27312	1.99903	4.26166	0.01243	6.27312
20	6	-0.23485	1.99912	4.22196	0.01378	6.23485
21	1	0.26384	0	0.73452	0.00164	0.73616
22	6	-0.2358	1.99912	4.22287	0.01381	6.2358
23	1	0.25686	0	0.74171	0.00143	0.74314
24	6	-0.25758	1.99911	4.24512	0.01335	6.25758
25	1	0.25409	0	0.74458	0.00133	0.74591
26	1	0.25371	0	0.74494	0.00135	0.74629
27	1	0.25247	0	0.74625	0.00129	0.74753
28	6	0.14797	1.99896	3.83416	0.01891	5.85203
29	6	-0.27312	1.99903	4.26167	0.01243	6.27312
30	6	-0.26139	1.99904	4.24922	0.01313	6.26139
31	6	-0.2358	1.99912	4.22287	0.01381	6.2358
32	1	0.25686	0	0.74171	0.00143	0.74314
33	6	-0.23486	1.99912	4.22196	0.01377	6.23486

34	1	0.26383	0	0.73453	0.00164	0.73617
35	6	-0.25759	1.99911	4.24512	0.01335	6.25759
36	1	0.25371	0	0.74494	0.00135	0.74629
37	1	0.25408	0	0.74459	0.00133	0.74592
38	1	0.25246	0	0.74625	0.00129	0.74754
39	7	-0.66034	1.99937	5.6425	0.01847	7.66034
40	7	-0.66014	1.99937	5.6423	0.01847	7.66014
41	31	1.57742	27.98315	1.42674	0.01269	29.42258
42	6	-1.29107	1.99954	5.27911	0.01243	7.29107
43	1	0.26431	0	0.73425	0.00143	0.73569
44	1	0.25345	0	0.74522	0.00133	0.74655
45	1	0.25466	0	0.74337	0.00196	0.74534
46	6	-1.29107	1.99954	5.27911	0.01243	7.29107
47	1	0.25344	0	0.74523	0.00133	0.74656
48	1	0.25467	0	0.74336	0.00196	0.74533
49	1	0.26431	0	0.73425	0.00144	0.73569

[a] Calculated at the level with PBE1PBE/6-31G(d,p)

Table S17. Summary of natural population analysis with ECP for **PhGaMe** in the gas phase[a]

Center Number	Atomic Number	Natural charge	Natural Population			
			Core	Valence	Rydberg	Total
1	6	-0.23933	1.99897	4.22633	0.01404	6.23933
2	6	-0.25736	1.99896	4.24463	0.01377	6.25736
3	6	-0.23933	1.99897	4.22633	0.01404	6.23933
4	6	-0.24931	1.99893	4.23734	0.01304	6.24931
5	6	-0.04228	1.99892	4.02822	0.01515	6.04228
6	6	-0.24931	1.99893	4.23734	0.01304	6.24931
7	1	0.25014	0	0.74824	0.00163	0.74986
8	1	0.24946	0	0.74895	0.00159	0.75054
9	1	0.25013	0	0.74824	0.00163	0.74987
10	1	0.24804	0	0.75015	0.0018	0.75196
11	1	0.24804	0	0.75015	0.0018	0.75196
12	6	-0.24553	1.99887	4.2302	0.01646	6.24553
13	6	0.1283	1.99903	3.85289	0.01979	5.8717
14	6	0.12829	1.99903	3.8529	0.01978	5.87171
15	1	0.23475	0	0.76283	0.00242	0.76525
16	1	0.23473	0	0.76285	0.00242	0.76527
17	6	0.14869	1.99881	3.83344	0.01906	5.85131
18	6	-0.26214	1.99891	4.24974	0.0135	6.26214
19	6	-0.27241	1.9989	4.26071	0.0128	6.27241
20	6	-0.23403	1.99897	4.22102	0.01403	6.23403
21	1	0.2627	0	0.73545	0.00185	0.7373
22	6	-0.23519	1.99897	4.22215	0.01407	6.23519
23	1	0.2562	0	0.74212	0.00168	0.7438
24	6	-0.25681	1.99897	4.24411	0.01373	6.25681
25	1	0.25348	0	0.74492	0.0016	0.74652
26	1	0.25302	0	0.74535	0.00163	0.74698
27	1	0.25178	0	0.74666	0.00156	0.74822
28	6	0.14871	1.99881	3.83342	0.01906	5.85129
29	6	-0.27242	1.9989	4.26072	0.0128	6.27242
30	6	-0.26212	1.99891	4.24972	0.0135	6.26212
31	6	-0.2352	1.99897	4.22216	0.01407	6.2352
32	1	0.2562	0	0.74213	0.00168	0.7438
33	6	-0.23404	1.99897	4.22103	0.01403	6.23404
34	1	0.26268	0	0.73546	0.00185	0.73732

35	6	-0.25682	1.99897	4.24412	0.01373	6.25682
36	1	0.25302	0	0.74535	0.00163	0.74698
37	1	0.25348	0	0.74492	0.0016	0.74652
38	1	0.25178	0	0.74666	0.00156	0.74822
39	7	-0.68295	1.99928	5.667	0.01666	7.68295
40	7	-0.68275	1.99928	5.6668	0.01666	7.68275
41	31	1.73828	28	1.25759	0.00413	29.26172
42	6	-1.3449	1.99944	5.3343	0.01116	7.3449
43	1	0.26252	0	0.73596	0.00152	0.73748
44	1	0.25177	0	0.74671	0.00152	0.74823
45	1	0.25431	0	0.74382	0.00187	0.74569
46	6	-1.3449	1.99944	5.3343	0.01116	7.3449
47	1	0.25176	0	0.74672	0.00152	0.74824
48	1	0.25432	0	0.74381	0.00187	0.74568
49	1	0.26252	0	0.73596	0.00152	0.73748

[a] Calculated at the level with PBE1PBE/6-31G(d,p) (for C, H, and N) and LanL2DZ (for Ga)

Table S18. Summary of natural population analysis with ECP for **PhInMe** in the gas phase[a]

Center Number	Atomic Number	Natural charge	Natural Population			
			Core	Valence	Rydberg	Total
1	6	-0.23924	1.99897	4.22631	0.01395	6.23924
2	6	-0.25637	1.99897	4.24372	0.01367	6.25637
3	6	-0.23924	1.99897	4.22631	0.01395	6.23924
4	6	-0.24904	1.99892	4.23699	0.01314	6.24904
5	6	-0.04138	1.99892	4.02704	0.01542	6.04138
6	6	-0.24904	1.99892	4.23699	0.01314	6.24904
7	1	0.24978	0	0.74859	0.00163	0.75022
8	1	0.24908	0	0.74932	0.00159	0.75092
9	1	0.24978	0	0.74859	0.00163	0.75022
10	1	0.24982	0	0.7484	0.00179	0.75018
11	1	0.24982	0	0.7484	0.00179	0.75018
12	6	-0.24682	1.99887	4.23118	0.01678	6.24682
13	6	0.12009	1.99903	3.86136	0.01951	5.87991
14	6	0.12009	1.99903	3.86136	0.01951	5.87991
15	1	0.23253	0	0.76494	0.00253	0.76747
16	1	0.23253	0	0.76494	0.00253	0.76747
17	6	0.14878	1.99881	3.83356	0.01885	5.85122
18	6	-0.27556	1.9989	4.26403	0.01263	6.27556
19	6	-0.26961	1.99891	4.25708	0.01363	6.26961
20	6	-0.23354	1.99898	4.22058	0.01398	6.23354
21	1	0.25567	0	0.74264	0.0017	0.74433
22	6	-0.23335	1.99898	4.22039	0.01398	6.23335
23	1	0.25818	0	0.74016	0.00166	0.74182
24	6	-0.25795	1.99897	4.2453	0.01368	6.25795
25	1	0.2527	0	0.74567	0.00163	0.7473
26	1	0.25325	0	0.74515	0.0016	0.74675
27	1	0.25128	0	0.74716	0.00156	0.74872
28	6	0.14878	1.99881	3.83356	0.01885	5.85122
29	6	-0.26961	1.99891	4.25708	0.01363	6.26961
30	6	-0.27556	1.9989	4.26403	0.01263	6.27556
31	6	-0.23335	1.99898	4.22039	0.01398	6.23335
32	1	0.25818	0	0.74016	0.00166	0.74182
33	6	-0.23354	1.99898	4.22058	0.01398	6.23354
34	1	0.25567	0	0.74264	0.0017	0.74433

35	6	-0.25795	1.99897	4.2453	0.01368	6.25795
36	1	0.25325	0	0.74515	0.0016	0.74675
37	1	0.2527	0	0.74567	0.00163	0.7473
38	1	0.25128	0	0.74716	0.00156	0.74872
39	7	-0.68018	1.9993	5.66547	0.0154	7.68018
40	7	-0.68018	1.9993	5.66547	0.0154	7.68018
41	49	1.74106	46	1.25589	0.00306	47.25894
42	6	-1.31029	1.99944	5.29883	0.01201	7.31029
43	1	0.25606	0	0.74244	0.00149	0.74394
44	1	0.24763	0	0.75083	0.00154	0.75237
45	1	0.2502	0	0.74805	0.00175	0.7498
46	6	-1.31029	1.99944	5.29883	0.01201	7.31029
47	1	0.24763	0	0.75083	0.00154	0.75237
48	1	0.2502	0	0.74805	0.00175	0.7498
49	1	0.25606	0	0.74244	0.00149	0.74394

[a] Calculated at the level with PBE1PBE/6-31G(d,p) (for C, H, and N) and LanL2DZ (for In)

Table S19. Distribution of HOMO and LUMO to each atom for **PhAlMe**[a]

Center Number	Atomic Number	Distribution	
		HOMO	LUMO
1	6	0.007163	0.005104
2	6	0.044293	0.000359
3	6	0.007154	0.005092
4	6	0.040835	0.013348
5	6	0.019126	0.052137
6	6	0.040818	0.013386
7	1	0.000426	2.28E-05
8	1	2.15E-05	0.000149
9	1	0.000426	2.29E-05
10	1	0.000532	0.004963
11	1	0.000532	0.00497
12	6	0.203982	0.004783
13	6	0.014341	0.215028
14	6	0.014394	0.214918
15	1	0.001491	0.000131
16	1	0.001449	0.000127
17	6	0.010082	0.026571
18	6	0.023099	0.021902
19	6	0.022874	0.021564
20	6	0.003656	0.003019
21	1	2.05E-05	0.003128
22	6	0.002062	0.006972
23	1	4.76E-05	0.000297
24	6	0.024402	0.024256
25	1	0.000349	0.000386
26	1	0.000338	0.000191
27	1	1.67E-05	8.2E-05
28	6	0.010114	0.026747
29	6	0.022965	0.021647
30	6	0.023189	0.022047
31	6	0.002075	0.007015
32	1	4.97E-05	0.000287
33	6	0.003658	0.003011
34	1	2E-05	0.003146

35	6	0.024561	0.024485
36	1	0.000335	0.000186
37	1	0.00035	0.000385
38	1	1.66E-05	8.18E-05
39	7	0.166623	0.118961
40	7	0.166675	0.118789
41	13	0.009907	0.002008
42	6	0.039685	0.001398
43	1	0.001109	0.001641
44	1	0.001448	0.0011
45	1	0.00033	5.3E-05
46	6	0.040032	0.001349
47	1	0.001504	0.001083
48	1	0.000326	5.22E-05
49	1	0.001096	0.001617

[a] Calculated at the level with PBE1PBE/6-31G(d,p)

Table S20. Distribution of HOMO and LUMO to each atom for **PhGaMe**[a]

Center Number	Atomic Number	Distribution	
		HOMO	LUMO
1	6	0.006944	0.00529
2	6	0.044032	0.000382
3	6	0.006942	0.005291
4	6	0.040937	0.013868
5	6	0.017348	0.054138
6	6	0.040939	0.013869
7	1	0.000417	2.4E-05
8	1	2.14E-05	0.000151
9	1	0.000417	2.4E-05
10	1	0.000513	0.005176
11	1	0.000513	0.005176
12	6	0.20944	0.004641
13	6	0.012577	0.212232
14	6	0.012549	0.212178
15	1	0.001647	0.000134
16	1	0.001646	0.000134
17	6	0.008984	0.026327
18	6	0.024543	0.020284
19	6	0.027053	0.027906
20	6	0.001845	0.004009
21	1	3.79E-05	0.000182
22	6	0.004342	0.003928
23	1	1.47E-05	0.004011
24	6	0.026141	0.029526
25	1	0.000361	0.000175
26	1	0.000306	0.000379
27	1	1.97E-05	0.000149
28	6	0.008996	0.026315
29	6	0.027064	0.027908
30	6	0.024554	0.02028
31	6	0.004345	0.003926
32	1	1.48E-05	0.004013
33	6	0.001847	0.004009
34	1	3.79E-05	0.000182

35	6	0.026163	0.029522
36	1	0.000305	0.000379
37	1	0.000361	0.000175
38	1	1.99E-05	0.000149
39	7	0.167479	0.109465
40	7	0.167462	0.109486
41	31	0.011045	0.010828
42	6	0.032661	0.001049
43	1	0.000961	0.000696
44	1	0.001356	0.000454
45	1	0.000795	7.89E-05
46	6	0.03266	0.001047
47	1	0.001353	0.000455
48	1	0.000795	7.84E-05
49	1	0.000962	0.000697

[a]Calculated at the level with PBE1PBE/6-31G(d,p)

Table S21. Distribution of HOMO and LUMO to each atom with ECP for **PhGaMe**[a]

Center Number	Atomic Number	Distribution	
		HOMO	LUMO
1	6	0.006791	0.00489
2	6	0.04438	0.00036
3	6	0.00679	0.004891
4	6	0.040811	0.01327
5	6	0.017751	0.049355
6	6	0.040807	0.013269
7	1	0.000412	2.26E-05
8	1	2.15E-05	0.000155
9	1	0.000412	2.27E-05
10	1	0.000497	0.005038
11	1	0.000498	0.005038
12	6	0.206503	0.004234
13	6	0.013414	0.210398
14	6	0.013384	0.210331
15	1	0.00168	0.000119
16	1	0.011094	0.02794
17	6	0.009778	0.028079
18	6	0.023113	0.021711
19	6	0.02526	0.023936
20	6	0.001764	0.006434
21	1	3.38E-05	0.000282
22	6	0.003996	0.003426
23	1	1.33E-05	0.003553
24	6	0.026184	0.028702
25	1	0.000347	0.000174
26	1	0.000336	0.000429
27	1	2.15E-05	9.16E-05
28	6	0.009789	0.028062
29	6	0.02527	0.023938
30	6	0.023127	0.021705
31	6	0.003996	0.003423
32	1	1.33E-05	0.003555
33	6	0.001765	0.006429
34	1	3.39E-05	0.000282

35	6	0.026207	0.028696
36	1	0.000335	0.000428
37	1	0.000346	0.000174
38	1	2.16E-05	9.17E-05
39	7	0.168919	0.116022
40	7	0.168908	0.116036
41	31	0.004127	0.001663
42	6	0.038116	0.002484
43	1	0.000691	0.002001
44	1	0.001278	0.001005
45	1	0.000154	8.91E-05
46	6	0.038103	0.002482
47	1	0.001275	0.001008
48	1	0.000154	8.9E-05
49	1	0.000692	0.002005

[a] Calculated at the level with PBE1PBE/6-31G(d,p) (for C, H, and N) and LanL2DZ (for Ga)

Table S22. Distribution of HOMO and LUMO to each atom with ECP for **PhInMe**[a]

Center Number	Atomic Number	Distribution	
		HOMO	LUMO
1	6	0.007133	0.005152
2	6	0.036756	0.00028
3	6	0.007133	0.005152
4	6	0.038002	0.012235
5	6	0.014944	0.04664
6	6	0.038002	0.012235
7	1	0.000499	1.89E-05
8	1	1.79E-05	0.00015
9	1	0.000499	1.89E-05
10	1	0.000588	0.00419
11	1	0.000588	0.00419
12	6	0.209221	0.0042
13	6	0.01251	0.209192
14	6	0.01251	0.209192
15	1	0.00151	0.000158
16	1	0.010677	0.030965
17	6	0.009541	0.031057
18	6	0.025997	0.025571
19	6	0.025921	0.022824
20	6	0.003434	0.003075
21	1	2.56E-05	0.003759
22	6	0.002486	0.007451
23	1	0.000201	0.000499
24	6	0.028934	0.030635
25	1	0.000303	0.000337
26	1	0.000292	0.000184
27	1	1.81E-05	8.56E-05
28	6	0.009541	0.031057
29	6	0.025921	0.022822
30	6	0.025997	0.025571
31	6	0.002486	0.007451
32	1	0.000201	0.000499
33	6	0.003434	0.003075
34	1	2.56E-05	0.003759

35	6	0.028934	0.030635
36	1	0.000292	0.000184
37	1	0.000303	0.000337
38	1	1.81E-05	8.56E-05
39	7	0.175956	0.114471
40	7	0.175956	0.114471
41	49	0.004421	0.001424
42	6	0.032568	0.001454
43	1	0.000486	0.00071
44	1	0.000701	0.000494
45	1	0.000214	0.000101
46	6	0.032568	0.001454
47	1	0.000701	0.000494
48	1	0.000214	0.000101
49	1	0.000486	0.00071

[a]Calculated at the level with PBE1PBE/6-31G(d,p) (for C, H, and N) and LanL2DZ (for In)

X-ray Diffraction Measurements

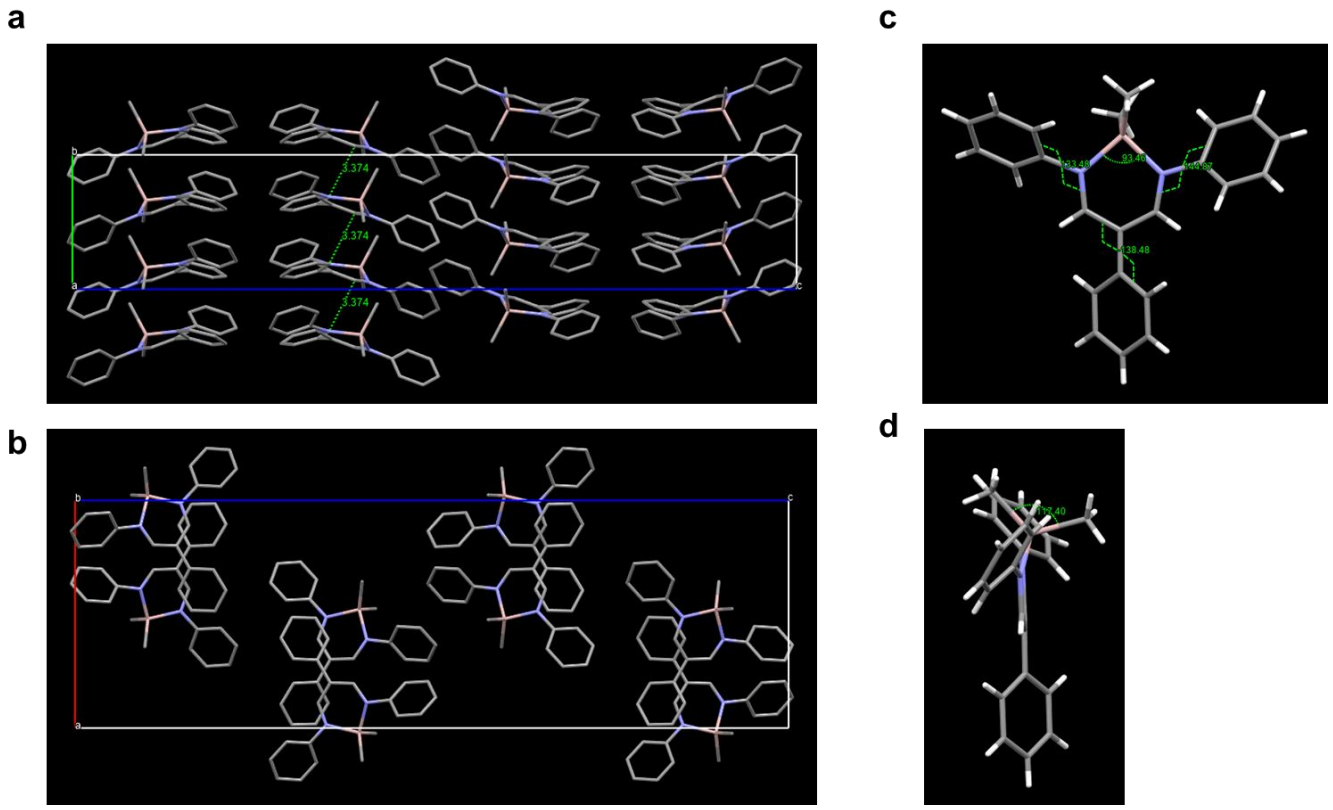

Figure S21. Packing structures of **PhAlMe** along with (a) *a* and (b) *b* axes. Selected (c) dihedral and (d) bond angles.

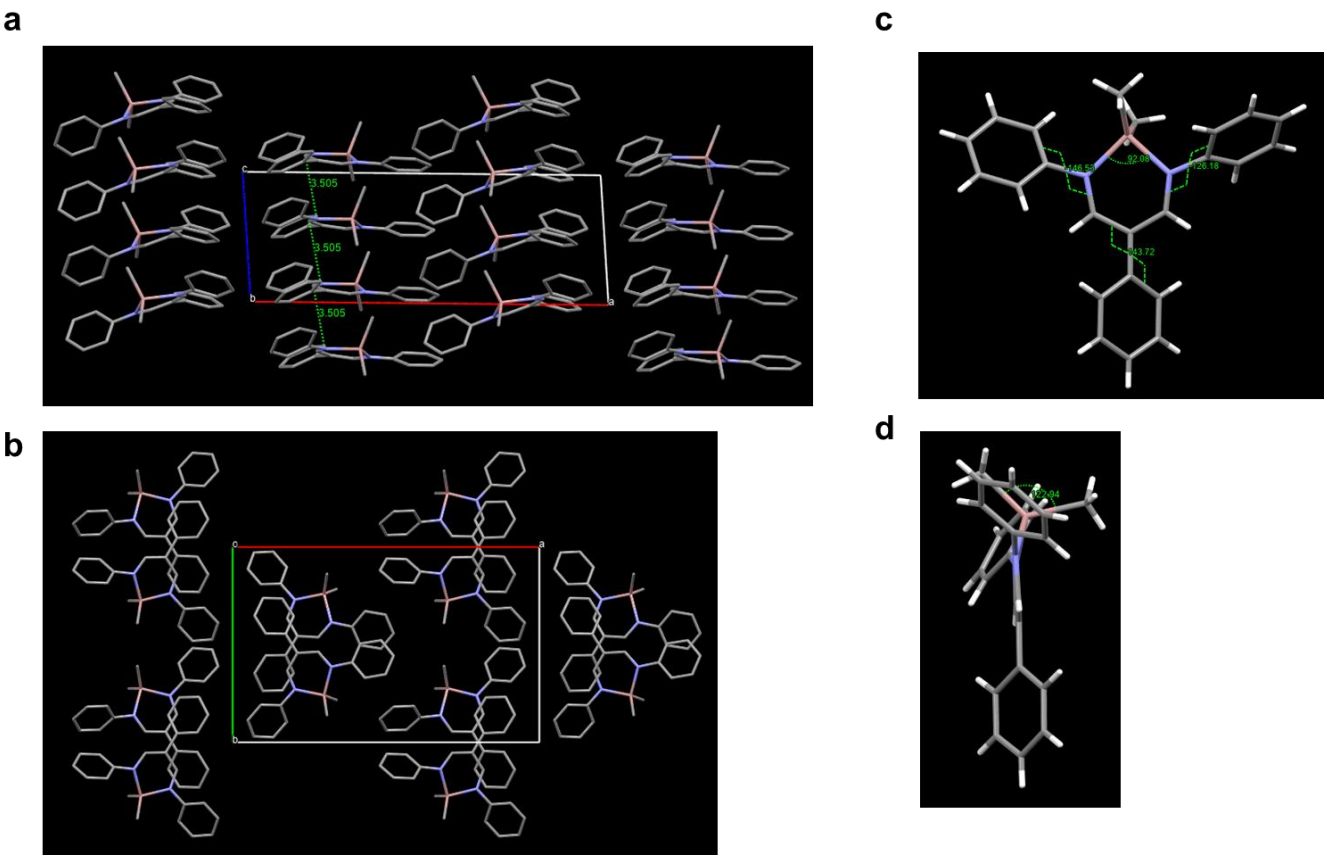

Figure S22. Packing structures of **PhGaMe** along with (a) *a* and (b) *b* axes. Selected (c) dihedral and (d) bond angles.

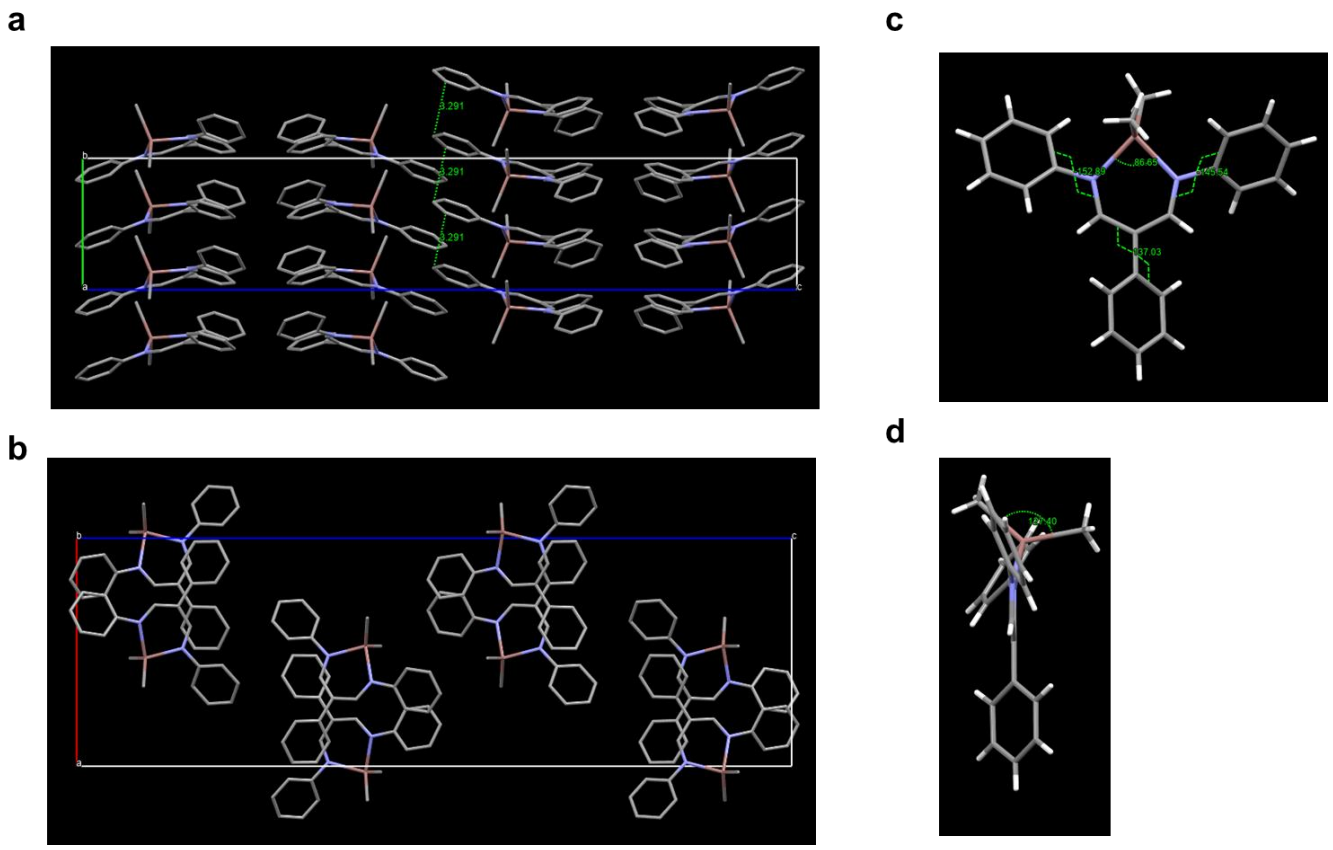

Figure S23. Packing structures of **PhInMe** along with (a) *a* and (b) *b* axes. Selected (c) dihedral and (d) bond angles.

Table S23. Crystallographic data of the complexes

parameters	PhAlMe	PhGaMe	PhInMe
CCDC Deposition No.	2245207	2245210	2245211
chemical formula	C23 H23 Al1 N2	C23 H23 Ga1 N2	C23 H23 In1 N2
formula weight	354.41	397.15	442.25
crystal system	orthorhombic	monoclinic	orthorhombic
space group	*Pbcn*	*Pc*	*Pbcn*
a (Å)	12.886(3)	20.397(9)	12.928(7)
b (Å)	7.5091(14)	12.948(6)	7.476(4)
c (Å)	40.514(8)	7.412(3)	40.60(2)
α (deg)	90	90	90
β (deg)	90	94.057(6)	90
γ (deg)	90	90	90
V (Å^3)	3920.2(14)	1952.8(15)	3924(4)
temperature (K)	150	150	150
Z	8	4	8
Radiation type	Mo $K\alpha$	Mo $K\alpha$	Mo $K\alpha$
ρ_{calc} (g cm^{-3})	1.201	1.351	1.497
μ (mm^{-1})	0.112	1.417	1.213
Crystal size	0.25 × 0.1 × 0.07	0.17 × 0.16 × 0.1	0.2 × 0.15 × 0.1
T_{min}, T_{max}	0.987, 0.992	0.786, 0.868	0.804, 0.886
2θ range (deg)	6.034 – 55.016	6.008 – 55.002	6.022 – 55.05
Reflections collected	24290	15731	18376
Independent reflections	4467	8112	4352
Observed reflections	4467	8112	4352
No. of parameters	237	473	237
R_{int}	0.0438	0.0773	0.0579
$R[I > 2\sigma(I)]$, wR_2	0.0528, 0.1264	0.0602, 0.1090	0.0354, 0.827
S	1.115	0.971	0.944

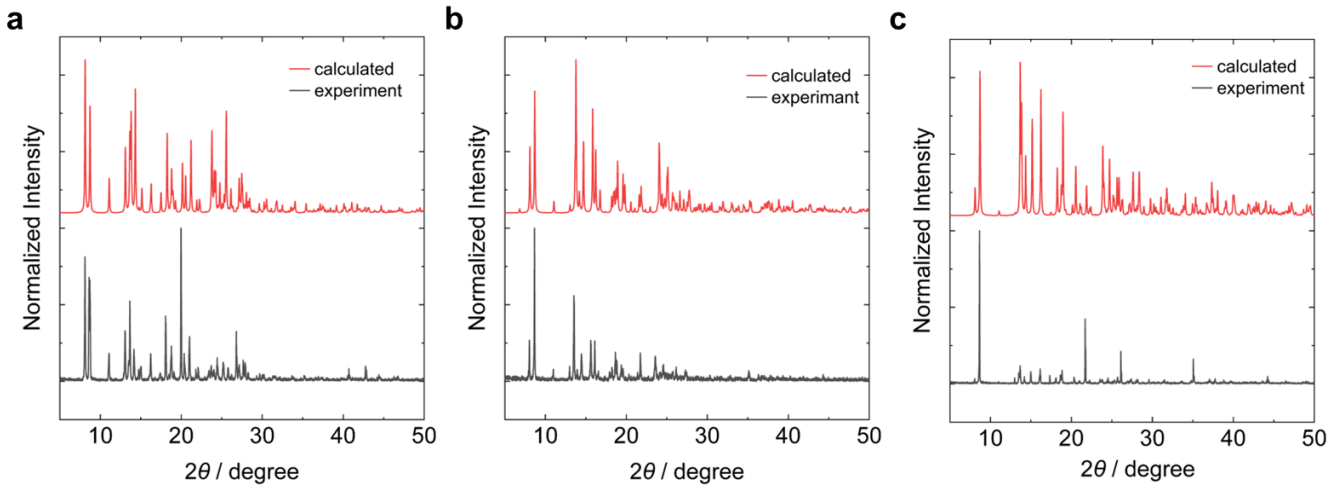

Figure S24. PXRD patterns of (a) **PhAlMe**, (b) **PhGaMe**, and (c) **PhInMe**. Red and black lines represent calculated profiles from the results of SCXRD analysis and experimental data, respectively.

References

[19] (a) Lippert, E. *Z. Naturforsch. A* **1955**, *10*, 541–545. (b) N. Mataga, Y. Kaifu, M. Koizumi, *Bull. Chem. Soc. J.* **1956**, *29*, 465–470.